



Application of machine learning to determine the shear stress and filtration loss properties of nano-based drilling fluid

Yee Cai Ning^{1,2} · Syahrir Ridha^{1,3} · Suhaib Umer Ilyas^{3,4} · Shwetank Krishna⁵ · Iskandar Dzulkarnain^{1,6} · Muslim Abdurrahman⁷

Received: 25 March 2022 / Accepted: 14 November 2022 / Published online: 16 December 2022
© The Author(s) 2022

Abstract

A detailed understanding of the drilling fluid rheology and filtration properties is essential to assuring reduced fluid loss during the transport process. As per literature review, silica nanoparticle is an exceptional additive to enhance drilling fluid rheology and filtration properties enhancement. However, a correlation based on nano-SiO₂-water-based drilling fluid that can quantify the rheology and filtration properties of nanofluids is not available. Thus, two data-driven machine learning approaches are proposed for prediction, i.e. artificial-neural-network and least-square-support-vector-machine (LSSVM). Parameters involved for the prediction of shear stress are SiO₂ concentration, temperature, and shear rate, whereas SiO₂ nanoparticle concentration, temperature, and time are the inputs to simulate filtration volume. A feed-forward multilayer perceptron is constructed and optimised using the Levenberg–Marquardt learning algorithm. The parameters for the LSSVM are optimised using Couple Simulated Annealing. The performance of each model is evaluated based on several statistical parameters. The predicted results achieved R^2 (coefficient of determination) value higher than 0.99 and MAE (mean absolute error) and MAPE (mean absolute percentage error) value below 7% for both the models. The developed models are further validated with experimental data that reveals an excellent agreement between predicted and experimental data.

Keywords Artificial neural network (ANN) · Drilling fluid · Filtration loss · Least square support vector machine (LSSVM) · Nanoparticles · Rheology

List of symbols

b	Bias value	w	Weight value
H_i	Hat matrix or projection matrix	x	Input data
T	Grubb's test critical value	X_i	Higher dimension value
i	Selected data index	y	Output value
i_n	Total input to a neuron	y_i^A	Original data
n	Number of data points	y_i^P	Predicted data
		φ	Mapping of input data

✉ Syahrir Ridha
syahrir.ridha@utp.edu.my

✉ Suhaib Umer Ilyas
suhaibui@gmail.com

Yee Cai Ning
cnyee@jadestone-energy.com

Shwetank Krishna
shwetank.krishna@unileoben.ac.at

¹ Petroleum Engineering Department, Universiti Teknologi PETRONAS, 32610 Seri Iskandar, Perak Darul Ridzuan, Malaysia

² Jadestone Energy Sdn Bhd, Menara IMC, No. 8, Jalan Sultan Ismail, 50250 Kuala Lumpur, Malaysia

³ Institute of Hydrocarbon Recovery, Universiti Teknologi PETRONAS, 32610 Seri Iskandar, Perak Darul Ridzuan, Malaysia

⁴ Department of Chemical Engineering, University of Gujarat, Jalalpur Jattan Road, Gujrat 50700, Pakistan

⁵ Department Petroleum Engineering, Chair of Drilling and Completion Engineering, Franz Josef-Straße 18, 8700 Montanuniversität, Leoben, Austria

⁶ Center of Research in Enhanced Oil Recovery, Universiti Teknologi PETRONAS, 32610 Seri Iskandar, Perak Darul Ridzuan, Malaysia

⁷ Petroleum Engineering Department, Universitas Islam Riau, Kota Pekanbaru 28284, Riau, Indonesia

γ	Regularisation parameter
σ	Kernel parameter to be optimised

Acronyms

ANN	Artificial neural network
API	American Petroleum Institute
CSA	Couple Simulated Annealing
FFMLP	Feed-forward multilayer perceptron
FL	Filtration loss
FV	Filtration Volume
GS	Gel strength
HPHT	High pressure high temperature
KKT	Karush–Kuhn–Tucker
LM	Levenberg–Marquardt
LSSVM	Least square support vector machine
MAE	Mean absolute error
MAPE	Mean absolute percentage error
MSE	Mean square error
NP	Nanoparticle(s)
PV	Plastic viscosity
R2	Regression coefficient
RMSE	Root mean square error
SS	Shear Stress
SVM	Support vector machine
WBM	Water-based mud
YP	Yield point

Introduction

The success of oil and gas well drilling operation is highly dependent on the selection and design of an appropriate drilling fluid. Generally, the expenditure of drilling fluid in a drilling operation ranges from 5 to 15%, but it may potentially cause significant drilling challenges (Smith et al. 2018; Agwu et al. 2018). The three main broad categories of drilling fluids are water-based mud (WBM), oil-based mud (OBM) and synthetic-based mud (SBM). WBM is commonly preferred amongst the other types due to its economic advantage, lower toxicity, and lower waste and environment challenges (Mahmoud et al. 2016; Smith et al. 2018). Drilling fluid has diverse functions in a drilling operation such as circulating drill cuttings and acting as the primary barrier for well control by exerting hydrostatic pressure on the formation. It also suspends the drill cuttings during a drilling break, cools and lubricates the drill bit, and maintains the wellbore stability in uncased section (Agarwal et al. 2011; Alvi et al. 2018).

Rheological properties of drilling fluid are critical to achieve an optimum drilling performance as it affects the hole cleaning process and rate of penetration in drilling (Gowida et al. 2019). Losing the basic required mud rheology such as plastic viscosity (PV), yield point (YP), and gel strength (GS) may lead to the occurrence of severe drilling complications

(Abdo and Haneef 2013). Drilling fluid that penetrates the permeable formation or the fluid loss will result in an invasion process and the formation of mud cake. It is crucial to mitigate an excessive fluid loss into formation as it will lead to formation of damage and affect the productivity and injectivity of a well (Contreras et al. 2014). Additives such as polymers and bentonite clay are commonly added in drilling fluid to function as a rheology modifier and fluid loss controller in drilling fluid. However, some weighting material and the polymeric additives tend to undergo degradation or breakdown at high-temperature condition, and it results in varying drilling mud rheology (Agarwal et al. 2011). According to Zakaria et al. (2012), conventional usage of a macro- or micro-drilling fluid often failed to reduce the fluid loss due to its size and limited functional ability.

Since the emergence of nanotechnology in the past decade, there were numerous experimental studies and research on the advantages of several nanoparticles on conventional drilling fluid. Silica (SiO₂) can be found abundantly in sand or quartz; it is one of the most commercialised nanoparticles due to its well-known preparation method (Riley et al. 2012). Recent research by Keshavarz Moraveji et al. (2020) showed that SiO₂ nanoparticles had improved the apparent viscosity, plastic viscosity and yield point of drilling mud compared to the base fluid. The thermal stability of the drilling fluid is improved proven by the less severe reduction in rheological behaviour after the hot rolling process in the presence of nanoparticles. The filtration loss (FL) of the drilling fluid also reduced with the increasing weight fraction of nanoparticles. A flow loop experiment conducted by Gbadamosi et al. (2019) using SiO₂ nanoparticle water-based drilling fluid demonstrated an improvement in borehole cleaning efficiency indicated by the increase in lifting efficiency of 13%. The enhancement in the drilling fluid rheology has enabled a better suspension and transport of cuttings to the surface. Mao et al. (2015) found that nanoparticle-assisted drilling fluid can effectively plug the micro-pores and micro-cracks through cross-linking and bridging. The formation of thin but dense mud cake aids to minimise the mud filtration loss as well as improve the pressure bearing capability of formation. Nanoparticles with ultra-fine sizes minimise the issue of accessing micropores or surfaces of the near-wellbore formations (Vryzas et al. 2015). According to Mao et al. (2015), SiO₂ in nano-scale exhibit high surface energy, rigidity, thermal and dimensional stability. It can function efficiently and effectively, along with the presence of other foreign molecules such as Acrylamide, sulfonic acid, Maleic anhydride, and Styren. Table 1 summarises the other applications of nanoparticles in the water-based drilling fluid. The effect of SiO₂ on drilling fluids had been extensively investigated showing positive results to rheological behaviour and filtration properties.

Recently, artificial intelligence (AI) has aroused attention and adaptability in the oil and gas industry. Machine learning,

Table 1 Previous studies of the application of nanoparticle in water-based drilling fluid

Author(s)	Nanoparticle (NP), average Size	Concentration	Conclusion
Medhi et al. (2020)	Zirconium Oxide (ZrO ₂) 27 nm	0–1.0 wt%	Increase in NP concentration improved the viscosity, elasticity and thermal stability with lesser filtrate loss
Vargas et al. (2020)	SiO ₂ 10–20 nm	0–0.1 wt%	Aside from the improvement in rheology, the addition of NP results in a reduction in filtration loss and mudcake thickness after the thermal ageing process
Aramendiz and Imqam (2020)	SiO ₂ 15–20 nm	0–1.0 wt%	Increase in PV, YP and GS with SiO ₂ NP up to 0.5 wt%. Further increase in concentration showed a reduction in YP and increase in FL, probably due to aggregation of NP
	Graphene (GNP) 15–20 nm	0–1.0 wt%	Increase in PV, YP and GS up to 0.2 wt% GNP. Further increase in GNP concentration above 0.4 wt% resulted in a little impact on GS and FL
Maiti et al. (2021)	SiO ₂	0–0.5 wt%	Positive effects shown in rheological properties, excellent imbibition effects on hydrate formation
Al-Yasiri and Wen (2019)]	Graphite–aluminium oxide (Gr-Al ₂ O ₃) 198 nm (Gr), 309 nm (Al ₂ O ₃)	0–0.8 wt%	Increase in PV and GS with shear-thinning behaviour captured. Thermal conductivity increased with increasing concentration
Alvi et al. (2018)	Boron Nitride (BN) 250 nm	0.05–2.0 g	No significant impact on FL and YP. Addition of 1.0 g BN showed most reduction in friction coefficient. Further increase in weightage increased friction coefficient
	Fe ₂ O ₃ 50nm	0.05–2.0 g	Addition of 0.05 g Fe ₂ O ₃ showed the most reduction in friction coefficient. YP increased, and no noticeable effect on FL
Cheraghian et al. (2018)	SiO ₂ 10nm	0.1–1.5 wt%	Increase in NP concentration improved the PV, YP, GS and reduced the thickness of mudcake
Sadegh Hassani et al. (2016)	SiO ₂	0.5 wt%	Increase in NP concentration improved the PV, AV, YP, and thermal stability
Kang et al. (2016)	SiO ₂ 150nm	0–10.0 wt%	Addition of SiO ₂ increased in PV and YP and a lower fluid loss. Higher NP concentration induced better physical plugging effect on the shale formation, which significantly decreased the imbibition amount, swelling rate and Young's modulus of the formation
Ghanbari et al. (2016)	SiO ₂ 10nm	0–0.5 wt%	Colloidal form of SiO ₂ increased the PV and YP of the drilling fluid with lower FL. The colloidal form of SiO ₂ proven to be more superior than the powder form due to a better dispersion technique
Cai et al. (2012)	SiO ₂ 5–20 nm	10 wt%	NP with size ranges from 7 to 15 nm are effective at plugging the pore throats of the shale formation. The penetration of the NP reduces the shale permeability, thereby minimised the interaction between shale and water-based fluid

as a subset of AI, is defined as a technique that is capable of processing multifaceted attributes from a historical database to deal with nonlinear problems for prediction and generalisation with high efficiency (Bello et al. 2015). As drilling is one of the most expensive operations in the industry, AI is reported in numerous studies as a proficient solution to reduce drilling cost (Bello et al. 2015). Artificial neural network (ANN), fuzzy logic, support vector machines (SVM), hybrid intelligent system (HIS), case-based reasoning (CBR) are some popular implementations in machine learning. According to the review by Agwu et al. (2018), both ANN and SVM have been utilised in the prediction of rheological properties and filtration loss with promising results. However, the

predictions performed only account for conventional drilling fluid without the inclusion of nanoparticles. Artificial neural network (ANN) was the first AI tool to be implemented in the oil and gas industry, and it is one of the most employed techniques of AI (Popa and Cassidy 2012). Other than the prediction of rheology and filtration loss, ANN has been applied in prediction of mud density, lost circulation, mudflow pattern, hole cleaning, cutting transport efficiency, settling velocity of cuttings and frictional pressure loss (Osman and Aggour 2003; Ozbayoglu and Ozbayoglu 2007; Al-Azani et al. 2019; Alkinani et al. 2020; Alanazi et al. 2022). The feed-forward multilayer perceptron (FFMLP) architecture, paired with a back-propagation learning algorithm, is the most widely used

ANN. Most networks comprised of one hidden layer adopting Levenberg–Marquardt (LM) as the optimisation method for weights and biases. The application of LM algorithm in ANN has demonstrated to outperform other algorithms such as Scaled Conjugate Gradient and Resilient Back-Propagation due to its fast and stable convergence (Sapna 2012; Du and Stephanus 2018; Yu and Wilamowski 2018; Liu et al. 2020). According to Yu and Wilamowski (2018), this algorithm is more robust and efficient in training small and medium-sized problem. It is noticeable that most of the predictions involve a conventional drilling fluid, and there are limited studies that involve the application of nanoparticles in drilling fluid. Table 2 shows the application of ANN in drilling fluids.

The application of LSSVM in the oil and gas industry is less prominent compared to the long-established ANN. Least square support vector machine (LSSVM), proposed by Suykens and Vandewalle in 1999, is an improvised machine learning approach of SVM that was developed by Cortes and Vapnik in 1995 (Chen et al. 2020). The SVM incorporates the idea of mapping nonlinear inputs from the primal to a higher dimensional space through a kernel function. The primary advantage of SVM compared to an ANN is that the computation process does not require hidden nodes, and it has fewer parameters to be optimised (Ghorbani et al. 2020). It has a better generalisation and a lower tendency to overfit. The quadratic programming algorithm in SVM involves variables subjected to linear constraints, commonly results in a more rapid convergence than ANN. However, SVM has a major downside due to its model complexity and required constrained optimisation programming that may cause a longer computation time (Wang and Hu 2005). The introduction of LSSVM has increased the efficiency and accuracy of a traditional SVM by using a sum-squared-error cost function which is a form of a linear system known as Karush–Kuhn–Tucker (KKT) instead of inequality constraints which is quadratic (Wang and Hu 2005; Asadi et al. 2021). Similar to SVM, LSSVM transforms the data from its defined dimension to a higher dimensional space to convert a nonlinear problem to be approximately linear (Ma et al. 2018). Radial basis function, also known as Gaussian, is the most capable and widely used kernel among the other kernels such as linear and polynomial. (Wang and Hu 2005; Ma et al. 2018; Uma Maheswari and Umamaheswari 2020). Table 3 summarises the studies of LSSVM in drilling operations.

Drilling fluid is a non-Newtonian fluid that violates the Newton's Law of Viscosity where the shear stress is not proportional to the shear rate applied. The rheology of a non-Newtonian drilling fluid can be described by the Bingham Plastic, Herschel–Bulkley and Power Law fluid model. The most widely used model, Bingham Plastic is a two-parameters rheological model. Based on a Bingham Plastic fluid shear stress versus shear rate graph, the intersection point depicts the yield point, and the slope represents the plastic viscosity

of a fluid. The pioneer analytical model to estimate the viscosity of mixtures or composites was developed by Einstein (1906). Modified models were proposed based on the Einstein model namely Brinkman model, Batchelor model and Graham model, mainly considering the interfacial layer on the nanoparticle (Udawattha et al. 2019). A correlation to determine nanofluid viscosity based on Brownian motion of nanoparticle developed in 2009, but it was contended to be negligible in 2016 (Masoumi et al. 2009; Moratis 2016). Researchers later started to discover the impact of temperature, size of particle, and concentration on viscosity through experiments (Udawattha et al. 2019). However, no exact correlation can provide the viscosity of nanofluids over a wide range of concentration. The static filtration behaviour of drilling fluid is determined through a static filter press test by applying a differential pressure at elevated temperature to simulate the borehole condition according to API specifications.

Mud formulations are often determined from laboratory experiments through trial and errors depending on the experience of the mud engineer to achieve the desirable properties (Shadravan et al. 2015). Laboratory experiments are time-consuming and expensive to conduct over a wide range of controlling parameters as it involves the preparation of base fluid and nanoparticles, dispersion and stabilisation of the nanoparticles in the solvent to achieve a favourable result (Shahsavari et al. 2019). Therefore, the incorporation of machine learning is essential in developing a system that utilises the available data and trends from past cases which will provide better insight for the mud engineer to increase efficiency and reduces the cost of experimenting. This research aimed to develop two machine learning models using ANN and LSSVM to predict the shear stress and filtration volume of SiO₂ nanoparticle water-based drilling fluid. The network performance for each prediction is evaluated by statistical parameters such as the coefficient of determination (R^2), root mean square error (RMSE), mean absolute percentage error (MAPE) and mean absolute error (MAE). The trend of predicted shear stress and filtration loss at varying input parameters is validated with the experimental trendline to gain intuition on the dependency of the outputs on the controlling factors.

Methodology

Data acquisition and normalisation

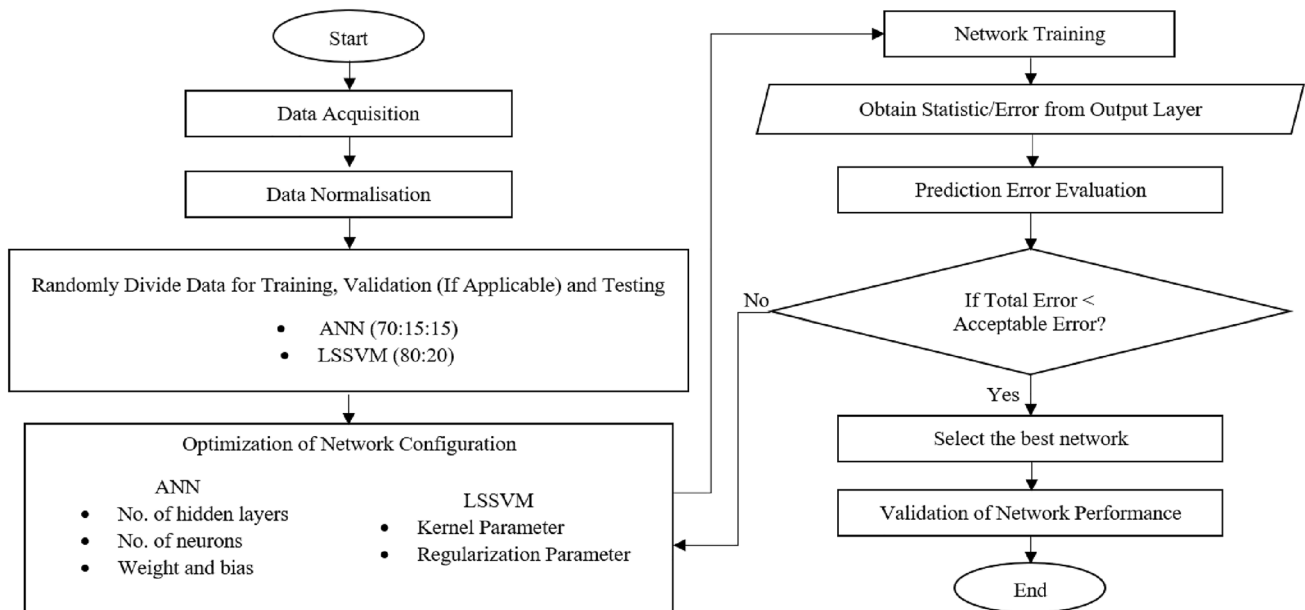
The foundation of a machine learning model is established based on historical data. To date, there are an appreciable number of experimental studies to examine the effect of SiO₂ nanoparticles on the properties of water-based drilling fluid with different variables. Figure 1 is the overall flowchart of the methodology adopted in this research work.

Table 2 Previous studies of ANN applications in drilling fluid

Author(s)	Type of prediction	ANN topology	Training function	Input	Output	Results
Gomaa et al. (2020)	Real-time rheological properties of high over-balanced WBM	FFMLP	LM	Mud weight, march funnel viscosity, plastic viscosity, yield point	Plastic viscosity, yield point, apparent viscosity, flow behaviour index, flow consistency index	AAPE = 7.7% $R^2 = 0.93$
Al-Khdheawi and Mahdi (2019)	Apparent viscosity of WBM	FFMLP	Gradient Descent (GD)	Marsh funnel viscosity, mud density	Apparent viscosity	$R^2 = 0.982$ AAE = 10.9%
Gowida et al. (2019)	Rheological properties of CaCl ₂ WBM	FFMLP	LM	Mud weight, Marsh funnel viscosity	Plastic viscosity, apparent viscosity, yield point, flow behaviour index, fluid consistency	$R^2 = 0.97-0.99$ AAPE = 2.4–3.9%
Golsefatan and Shahbazi (2021)	Filtration volume of SiO ₂ NP in WBM	FFMLP	LM	Temperature, time, NP concentration, KCl salt concentration	Filtration volume	$R^2 = 0.9928$ RMSE = 0.6926 AAE = 2.6636% ARE = 0.1361%
Tomiwa et al. (2019)	Rheology properties of a Solanum tuberosum formulated biopolymer improved WBM	FFMLP	LM	Quantity of bentonite and solanum tuberosum biopolymer	Apparent viscosity, plastic viscosity, yield point	RMSE = 1.2522 $R^2 = 0.9937$
Bispo et al. (2017)	Apparent viscosity of WBM	FFMLP	LM	Temperature, concentration of barite, bentonite and xanthan gum	Apparent viscosity	Relative error within 10%
Barati-Harooni et al. (2016)	Frictional pressure loss for two-phase gasified drilling fluid with cuttings in an inclined annulus	(Radial Basis Function) FFRBF	Genetic Algorithm (GA)	Gas and liquid superficial velocity, pipe rotation speed, rate of penetration, hole inclination	Frictional pressure loss	$R^2 = 0.9965$ AARD = 2.1667 RMSE = 0.0088
Maghrabi et al. (2014)	Erosion behaviour of shale cuttings in WBM	FFMLP	N/A	Shale mineralogy and fluid composition	Percentage of shale recovery	$R^2 = 0.85-0.90$ RMSE = 7.6 to 9.2
Safari et al. (2014)	Hole cleaning efficiency of foam drilling mud	FFMLP	Bayesian Regularisation (BR)	Temperature, pressure, pipe rotation, foam quality and velocity, annulus eccentricity	Cutting's concentration	$R^2 = 0.914-0.994$ AAPE = 2.38–5.93%

Table 3 Previous studies of LSSVM applications in oil and gas industry

Author(s)	Type of prediction	Type of optimisation	Input	Output	Results
Asadi et al. (2021)	Dynamic viscosity of MWCNT-MgO/oil hybrid nanofluid	Bayesian Optimisation	Temperature, NP concentration, shear rate	Dynamic viscosity of oil hybrid nanofluid	MSE = 1.161 $R^2 = 0.999$
Golsefatan and Shahbazi (2021)	Filtration volume of SiO ₂ NP in WBM	Couple Simulated Annealing (CSA)	Temperature, time, NP concentration, KCl salt concentration	Filtration volume	$R^2 = 0.994$
Ahmadi (2016)	Drilling fluid density of OBM, WBM and SBM	Genetic Algorithm	Pressure, temperature	Mud density	MSE = 0.000145 $R^2 = 0.999$
Meybodi et al. (2015)	Viscosity of Al ₂ O ₃ , TiO ₂ , SiO ₂ , CuO water-based nanofluids	CSA	NP type, size, concentration, temperature	Viscosity of nanofluid	RMSE = 3.7084 AARE = 2.144% $R^2 = 0.9979$
Tanoumand et al. (2015)	Viscosity of Diluted Heavy Oil in Presence of Kerosene	CSA	Temperature, kerosene mass fraction	Viscosity	RMSE = 516.33 $R^2 = 0.999$ MAPE = 1.89%
	Frictional pressure loss in a 3-phase flow (drilling fluid, air, cuttings)	CSA	In situ flow rate of each phase, rate of penetration, pipe rotation, hole inclination	Frictional pressure loss	RMSE = 0.018 $R^2 = 0.9862$ AARD = 3.459%
Milad Arabloo (2014)	Frictional pressure loss for multiphase flow in inclined annuli	CSA	Gas and liquid superficial velocity, pipe rotation speed, rate of penetration, hole inclination	Frictional pressure loss	$R^2 = 0.9862$ AARD = 3.459 RMSE = 0.018

**Fig. 1** General workflow to develop the machine learning models

The input parameters utilised for the prediction of shear stress include shear rate, nanoparticle concentration and temperature. One hundred fifty-six (156) data points are gathered from three (3) published experimental results

(Vryzas et al. 2015; Mahmoud et al. 2016, 2018). The WBM formulation for all the studies contained seven (7) wt% bentonite prepared according to the requirement of API Specifications 13A. The nano-silica used in all studies had

Table 4 Statistical description of databank for prediction of shear stress

Parameter	Minimum	Maximum	Mean	Standard deviation
Nanoparticle Concentration (wt%)	0	2.5	0.996	0.841
Temperature (°F)	78	200	136.448	33.564
Shear rate (1/s)	4.81	1027.47	312.054	338.362
Shear Stress (lbf/100ft ²)	0	200	312.054	14.758

Table 5 Statistical description of databank for prediction of filtration volume

Parameter	Minimum	Maximum	Mean	Standard deviation
Nanoparticle Concentration (wt%)	0	7.5	3.257	2.738
Temperature (°F)	77	199	134.189	45.887
Time (s)	2.52	1801.90	583.775	555.786
Filtration Volume (ml)	1.679	30.204	10.053	5.717

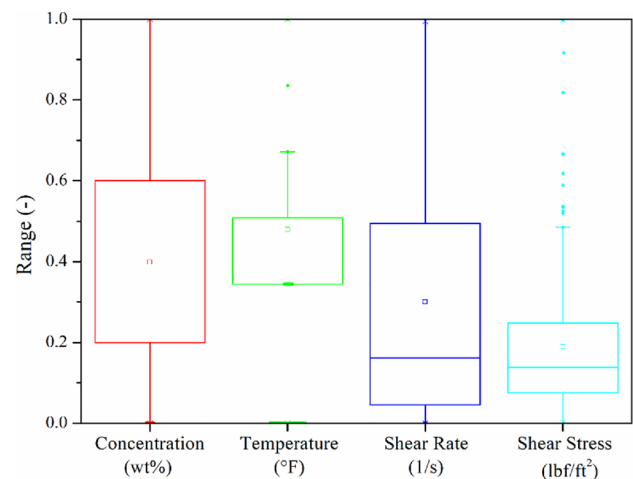
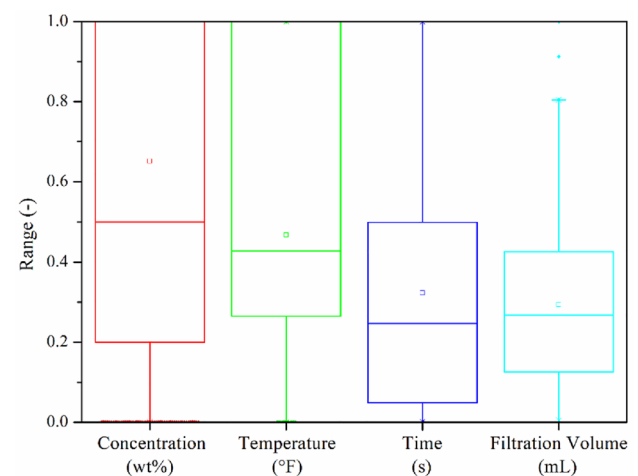
an average size of 12 nm. The experiment was conducted at varying nanoparticles concentration from 0 to 2.5 wt% and temperature from 78 °F to 200 °F at atmospheric pressure. The shear stress of the drilling fluid was measured at shear rates ranges in 4 s^{-1} to 1200 s^{-1} .

Two hundred fifty-four (254) data points comprised of nanoparticle concentration, temperature and time from another published literature have contributed as the inputs for the prediction of filtration loss (Parizad et al. 2018). The average grain size for the SiO_2 nanoparticles used in this research range from 10 to 15 nm. The filtration loss of SiO_2 nanoparticle drilling fluid was measured by conducting API filtration test at a varying concentration from 0 to 7.5 wt% and temperature from 77 °F to 199.4 °F at a fixed differential pressure of 100 psig. The filtration volume was recorded at a different interval within 30 min. Tables 4 and 5 are the statistical descriptions of the datasets for the prediction of shear stress and filtration volume, respectively.

All data parameters are normalised based on the minimum and maximum value according to Eq. (1). Data normalisation is a good practice prior to training to adjust the data distribution so that the mean of all data points is close to zero (Razi et al. 2013; Liu et al. 2020). Normalised data can increase the efficiency of training and speed up the network convergence. The illustrations of data distribution for prediction of shear stress and filtration loss after normalisation are shown in Fig. 2 and Fig. 3, respectively.

The data points marked beyond the minimum and maximum line indicate the outliers. Generally, the filtration loss datasets have a better quality than shear stress as there were ten (10) outliers out of 156 data of experimental shear stress values. For the experimental of filtration loss, there were only two (2) outliers out of 254 data points.

$$x'_n = \frac{x - x_{\min}}{x_{\max} - x_{\min}} \quad (1)$$

**Fig. 2** Distribution of normalised data for prediction of shear stress**Fig. 3** Distribution of normalised data for prediction of filtration loss

Artificial neural network (ANN)

Every artificial neuron comprises multiplication, summation and activation function represented by the mathematical model in Eq. 2. Multiple artificial neurons must be combined to harvest the capability of an ANN completely. There are several possible ways to connect the neurons, and the terminology to describe the interconnection of neurons is known as topology or architecture. A multilayer feed-forward ANN architecture where information generally flows in a forward direction from input to output is employed in this research. The activation function for the input layer and hidden layers follows the nonlinear function, whereas the linear activation function is selected for the output layer to assure the outcome to be in the acceptable range. Tansig (Hyperbolic tangent sigmoid function) is employed as an activation function for input and hidden layer, and Purelin (Linear

transfer function) is used as an activation function for the output layer. Figure 4 and Fig. 5 illustrate the architecture of ANN for the prediction of shear stress and filtration loss, respectively.

$$y = F\left(\sum_{i=0}^n w_i \cdot x_i + b\right) \quad (2)$$

where y is the output, x is the input, w is the weight, b is the bias, i is the data index, and n is the total number of data points. The initial weight of the ANN model is selected randomly in the range of $\left(\frac{-1}{\sqrt{i_n}}, \frac{1}{\sqrt{i_n}}\right)$, where ' i_n ' is the total input to a neuron.

ANN model may consist of single or multiple hidden layers depending on the complexity of the problem and optimisation process. The presence of hidden layers with neurons provides an extrasynaptic connection and dimension of

Fig. 4 ANN architecture for prediction of shear stress

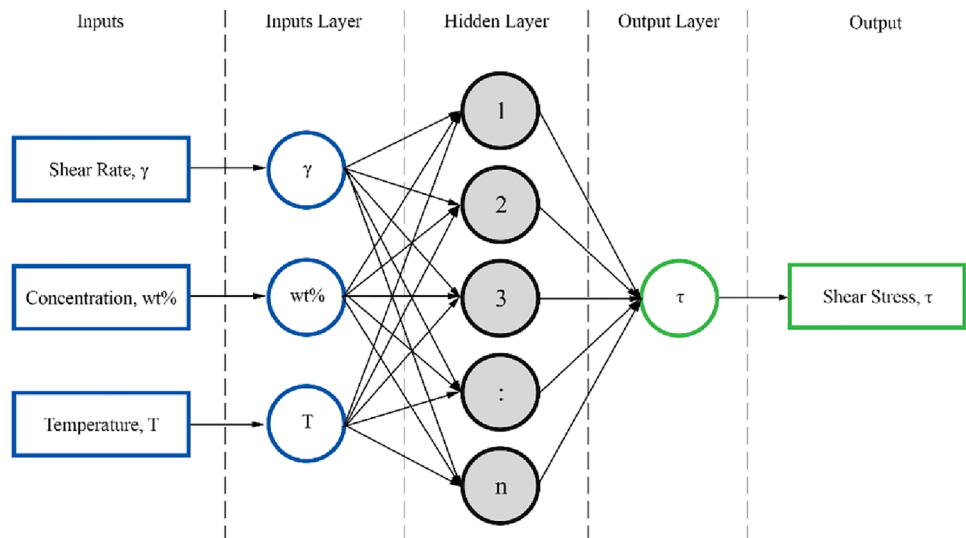
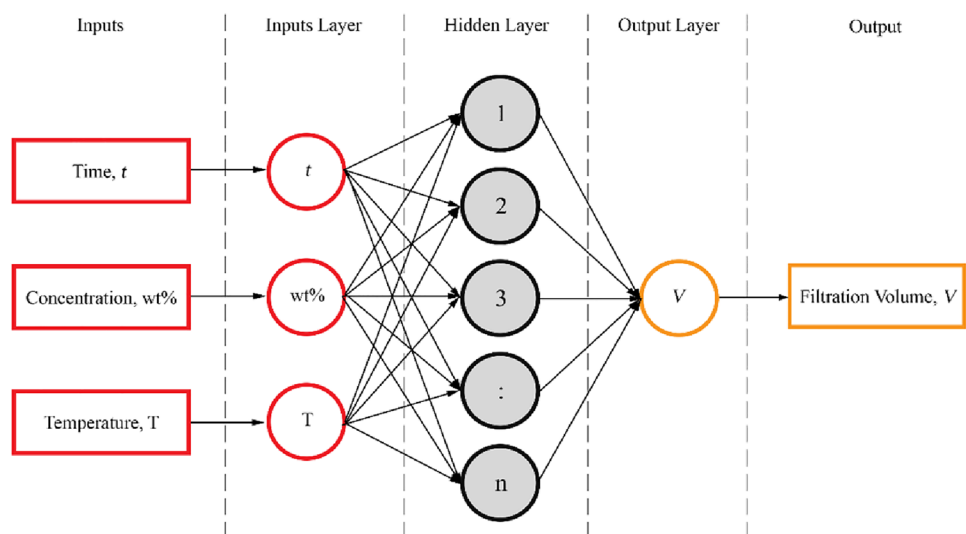


Fig. 5 ANN architecture for prediction of filtration volume



neural interactions (Cohen 1994). A trial-and-error approach by manipulating the number of hidden layers and neurons is adopted to finalise a topology best suited for the predictions. The loss/error function is set to the root mean square error (RMSE). The RMSE depicts the error in the new developed model by indicating the deviation between actual data and predicted data. This error is used to evaluate and compare the different ANN architecture with varying neurons and hidden layer to determine the best topology. An optimal number of neurons in the hidden layers is vital to avoid underfitting or overfitting due to excessive or insufficient neurons. A back-propagation learning algorithm Levenberg–Marquardt is used to optimise the weights and biases. The entire model is established using a simulation tool, MATLAB (R2020a).

The proportion of the training, validation, and testing vectors for the construction of ANN to predict shear stress and filtration volume is 70:15:15 and 80:10:10, respectively. The validation datasets act as the stopping criteria of a training process. The network training will halt if the performance of the validation samples failed to improve or remains for six (6) consecutive epochs in a row. Mean square error (MSE) is the indicator of the improvement in the prediction.

Least square support vector machine (LSSVM)

The LSSVM network has a simpler architecture as it involves fewer tuning parameters and no hidden nodes involved compared to ANN. According to Asadi et al. (2021), the linear form of the input and output vectors in an LSSVM model can be generally represented by Eq. 3 where φ is the mapping of inputs, X_i to a higher dimension. The weight, W and bias, b are determined from the cost function in Eq. 4 in which a regularisation parameter, gamma (γ), is involved. A final form of LSSVM is shown in Eq. 5 which K features the kernel trick to be applied in the LSSVM model. Radial basis function will be the kernel trick in this research, and it is formulated in Eq. 6, where sigma (σ) is the kernel parameter to be optimised.

$$y_i = w^T \cdot \varphi(y_i) + b \quad (3)$$

$$\text{CostFunction} = \frac{1}{2} w^T w + \frac{\gamma}{2} \sum_{i=1}^n e_i^2 \quad (4)$$

$$y_i = \sum_{i=1}^n a_i K(x_i \cdot x_j) + b \quad (5)$$

$$K(x_i \cdot x_j) = \exp \left[-\frac{|x_i - x_j|^2}{2\sigma^2} \right] \quad (6)$$

The proportion of training for the testing dataset in the LSSVM model to predict shear stress and filtration volume

has a ratio of 80:20 and 70:30, respectively. The tuning parameters, which includes the kernel (σ^2) and regularisation (γ) parameter, are optimised by the Couple Simulated Annealing (CSA) algorithm. CSA is a modified technique from simulated annealing (SA) that exhibits a higher convergence speed and accuracy (Dashti et al. 2020; Ghorbani et al. 2020). The best-optimised parameters are finalised after an iterative process of training, testing and performance evaluation. Figure 6 and Fig. 7 exhibit the LSSVM architecture for prediction of shear stress and filtration volume, respectively.

Model performance evaluation

The statistical parameters used to evaluate the performance or accuracy of the network are the coefficient of determination (R^2), root mean square error (RMSE) and mean absolute percentage error (MAPE) and mean absolute error (MAE). These values are computed for all the predicted output from training, validation and testing. R^2 measures how close the outputs are fitted to the target values. RMSE, MAPE and MAE depict the difference between the experimental and predicted values. R^2 value close to 1 or a low value of RMSE, MAPE and MAE indicates a favourable prediction result. R^2 , RMSE, MAPE and MAE are expressed mathematically as Eq. (7) to (10), respectively, where, y_i^A is the original used data and y_i^P is the predicted data.

$$R^2 = 1 - \frac{\sum_{i=1}^{i=n} (y_i^A - y_i^P)^2}{\sum_{i=1}^{i=n} (y_i^{\text{Actual}} - \bar{y})^2} \quad (7)$$

$$\text{RMSE} = \sqrt{\frac{1}{n} \sum_{i=1}^{i=n} (y_i^A - y_i^P)^2} \quad (8)$$

$$\text{MAPE}(\%) = \frac{100}{n} \sum_{i=1}^{i=n} \left| \frac{y_i^A - y_i^P}{y_i^{\text{Actual}}} \right| \quad (9)$$

$$\text{MAE} = \frac{1}{n} \sum_{i=1}^{i=n} |y_i^A - y_i^P| \quad (10)$$

Results and discussion

Prediction of shear stress

Artificial neural network (ANN)

Twenty (20) iterations were performed by manipulating the number of the hidden layer(s) from 1 to 2 and the number of hidden node(s) from 1 to 50. The network configuration with the lowest overall RMSE is the optimum network architecture, and its topology will be selected for further prediction. Figure 8 plots the RMSE of the predicted training, validation

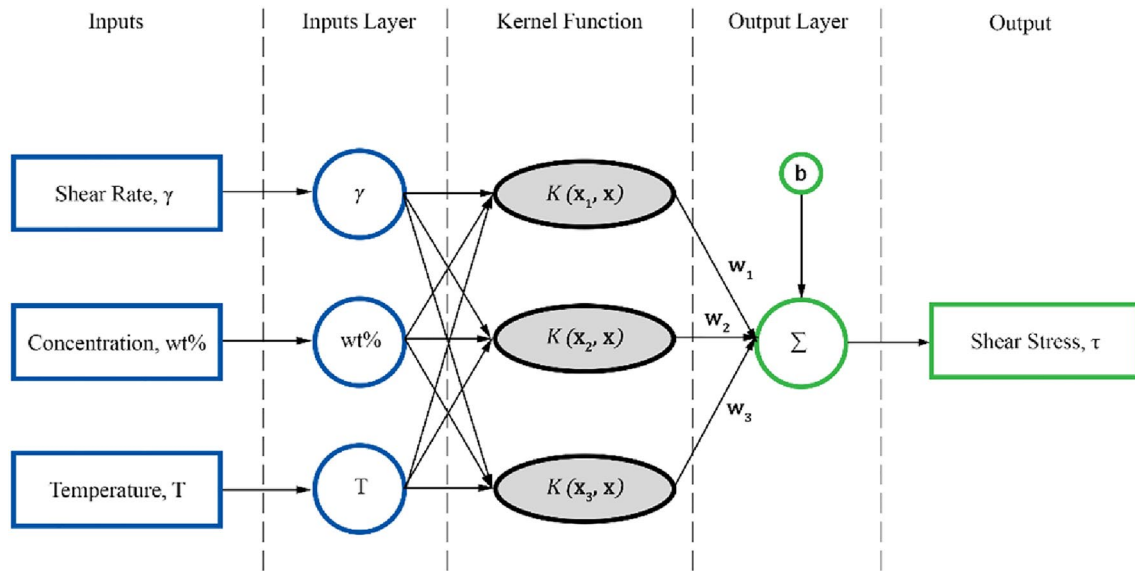


Fig. 6 LSSVM architecture for prediction of shear stress

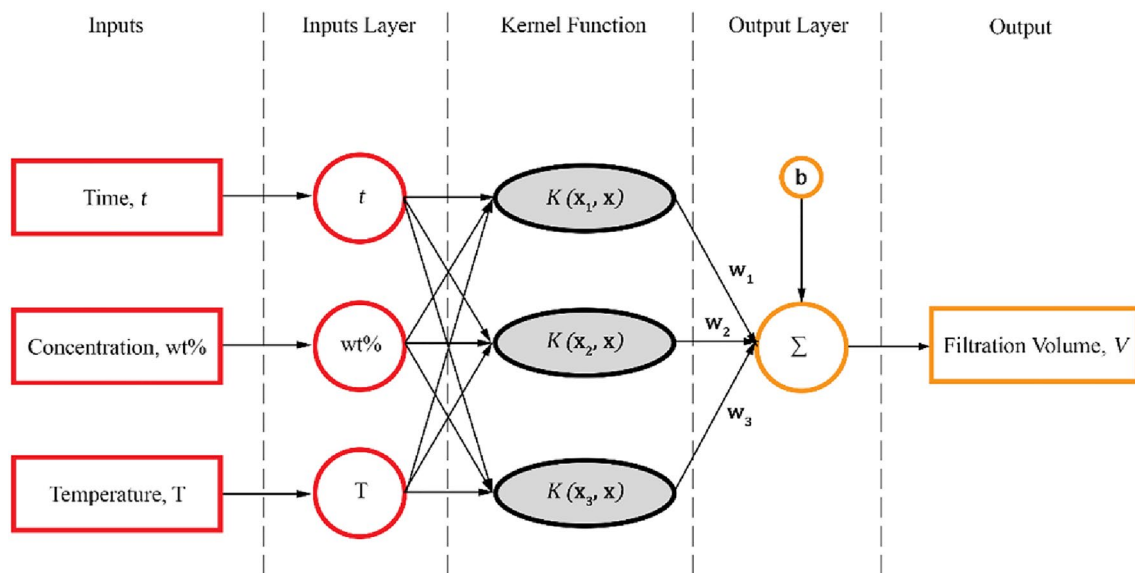


Fig. 7 LSSVM architecture for prediction of filtration volume

and testing outputs obtained from the best iteration. Based on the plots, the increase in neurons does not guarantee an increase in accuracy as weight and biases are continually changing in every run. Table 6 quantifies the RMSE and R^2 of the best quantity of hidden neuron(s) using 1 and 2 hidden layer(s). The overall RMSE and R^2 values are averaged from the RMSE and R^2 values of training, validation and testing vectors. A well-tuned model should be capable of yielding high accuracy for the prediction of all the training, validation and testing vectors without jeopardising the accuracy of one another. Based on Table 6, one (1) hidden layer generally

performed better than the two (2) hidden layers networks as it has a lower RMSE and higher R^2 values. The best performance is achieved with one (1) hidden layer consisting of 18 hidden nodes with an overall RMSE of 2.0235 lbf/ft² and R^2 of 0.9924. Therefore, a topology of 3–18–1 is selected for the prediction of shear stress.

The weights and biases of every neuron optimised by LM algorithm are extracted from the finalised network configurations for further training, validation and testing process. Figure 9 shows the MSE at every epoch for the prediction of shear stress. Epoch is the measure of how many times

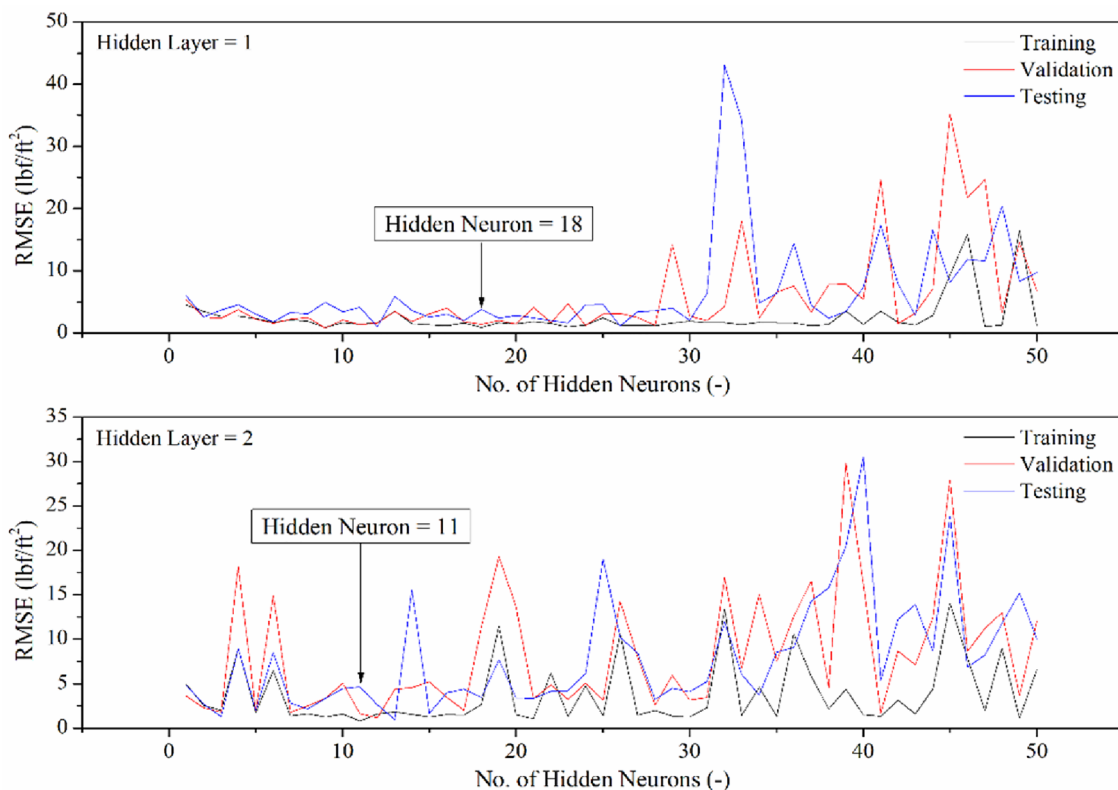


Fig. 8 RMSE of ANN for prediction of shear stress

Table 6 Statistics of ANN predicted shear stress for 1 and 2 hidden layers

Hidden Layer	Prediction of shear stress	
	1	2
Iteration	15	16
Hidden Neurons	18	11
RMSE (Training), lbf/ft ²	0.8931	0.7885
RMSE (Validation), lbf/ft ²	1.3780	1.6145
RMSE (Testing), lbf/ft ²	3.7993	4.6384
R ² (Training)	0.9983	0.9984
R ² (Validation)	0.9930	0.9935
R ² (Testing)	0.9860	0.9737
Overall RMSE, lbf/ft ²	2.0235	2.3471
Overall R ²	0.9924	0.9885

the training vectors are passed back from the output layer to update the weights and biases. The best result for the validation dataset is achieved at zeroth epoch with the lowest MSE of 0.24453 lbf/ft². Since there is no noticeable improvement for six (6) consecutive epochs, the stopping criterion is triggered, and the training cycle is ceased. Based on Fig. 9, MSE for all the train, validation and test vectors stabilises after the

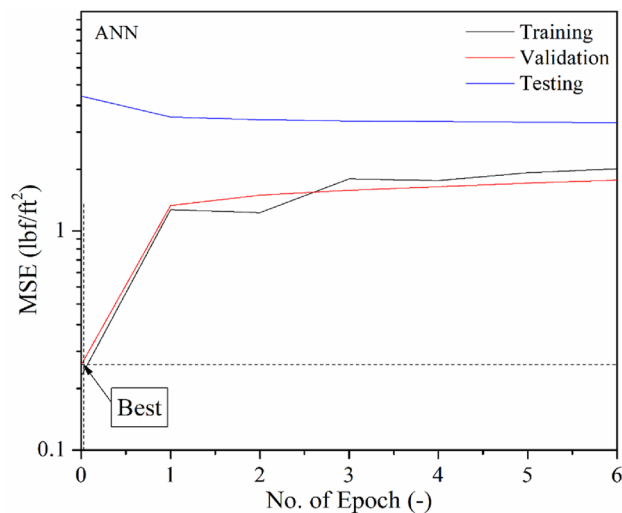


Fig. 9 MSE at different epochs of ANN for prediction of shear stress

fourth epoch, this is where the network found the optimal solution for the weights and biases.

Figure 10 shows the parity plots of the predicted outputs versus actual shear stress. The training, validation and testing R² values are 0.993, 0.998 and 0.999, respectively. The coefficient of determination of both test and validation

vectors exceeds 0.995, although training data sets yield a slightly lower value. The R^2 infers that the network has an excellent generalisation to the new testing data points and does not overfit. The calculated RMSE based on the predicted and experimental outputs from training, validation, testing is 2.029 lbf/ft², 0.495 lbf/ft², and 0.466 lbf/ft².

A graphical plot of the error distributions is presented in Fig. 11 to demonstrate the error in the prediction of the developed ANN model. Based on the plot, the maximum relative error between the predicted and actual shear stress ranges from about -40 to 30%.

Least square support vector machine (LSSVM)

Twenty (20) iterations with 100 runs each were performed to determine the radial basis function kernel parameter (σ) and regularisation parameter (γ). These parameters are initialised randomly and optimised by CSA. The best performance from each iteration is ranked based on the lowest RMSE, and the results are plotted in Fig. 12. Based on the figure, the 16th iteration yields the lowest overall RMSE with a value of 1.452 lbf/ft². The kernel and the regularisation parameters

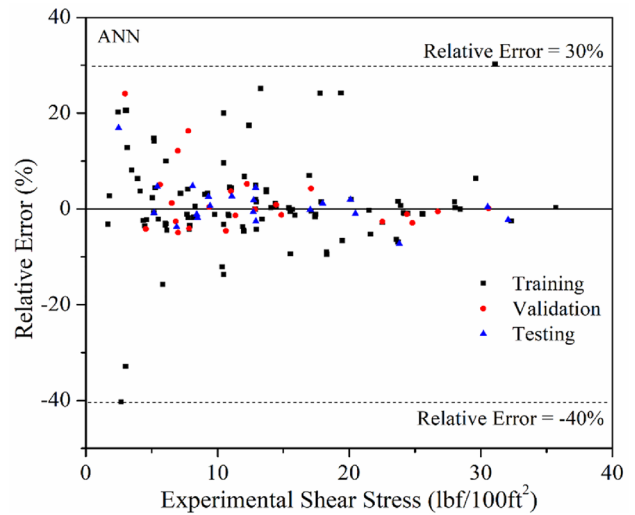


Fig. 11 Relative error of ANN for prediction of shear stress

are acquired from the optimal iteration with the values of 1.5706e+05 and 13.5046.

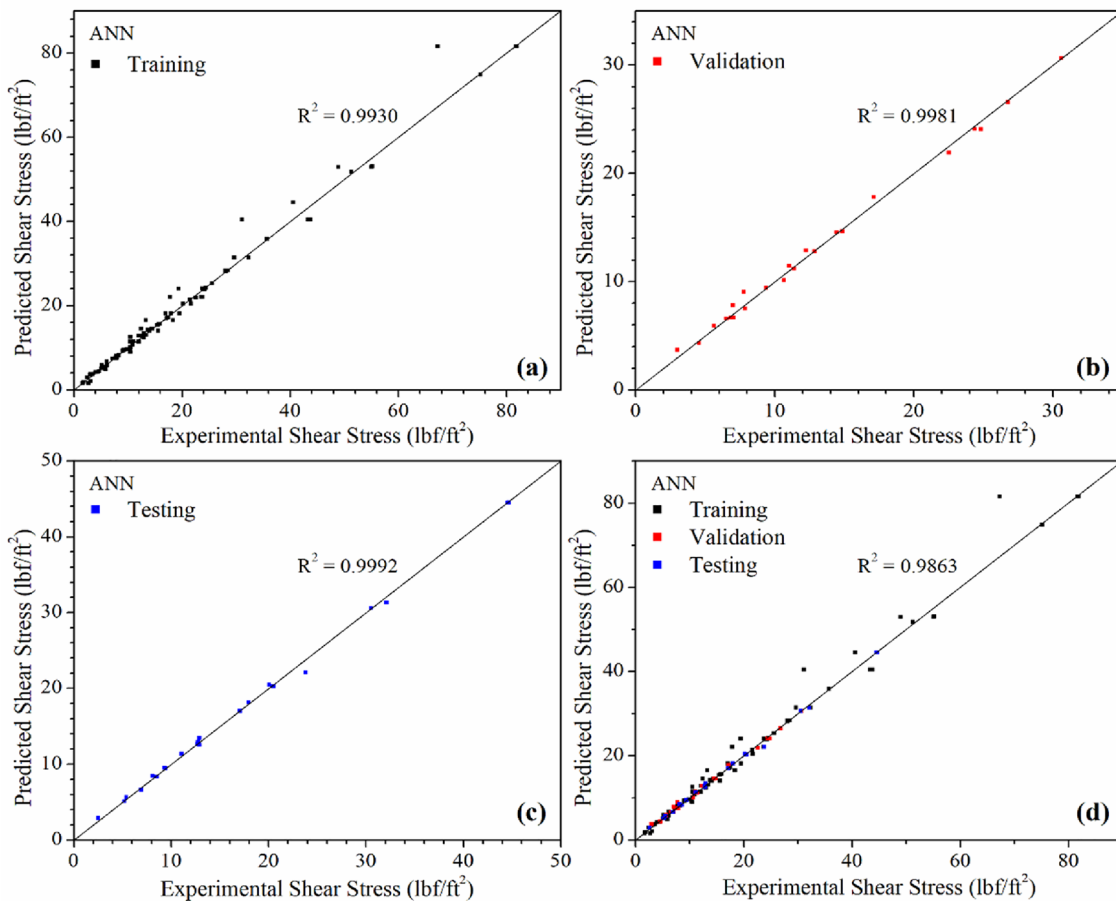


Fig. 10 Parity plots of ANN for prediction of shear stress: **a** Overall Data **b** Training Data **c** Validation Data **d** Testing Data

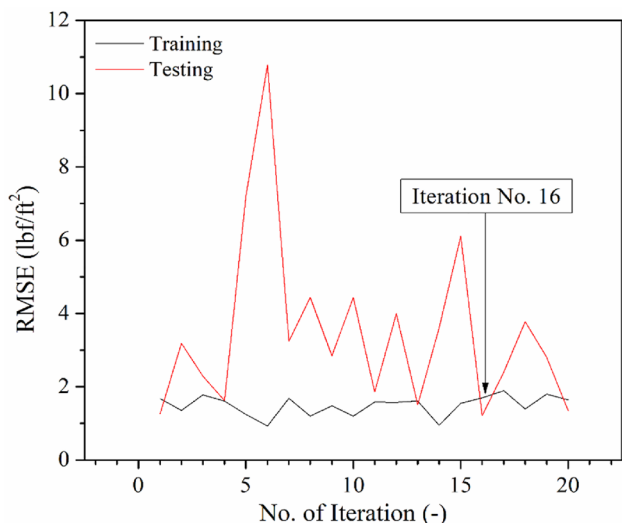


Fig. 12 RMSE of LSSVM for prediction of shear stress

The RMSE of prediction of shear stress for training and testing datasets is 1.696 lbf/ft² and 1.209 lbf/ft². Figure 13 (a–c) shows the parity plots for the training and testing vectors of prediction of filtration volume with R^2 of 0.994 and 0.995, respectively. The R^2 values, which are very close to 1.0, demonstrate the capability of LSSVM to predict the shear stress accurately. The reasonably low RMSE and high R^2 of testing datasets proved the model has a low tendency to overfit the training vectors. The relative error is plotted in Fig. 13 (d). The predicted output deviates with a maximum relative error from –18.2 to 26.8%.

Prediction of filtration volume

Artificial neural network (ANN)

The methodology to determine the architecture for prediction of filtration loss is similar to the approach in prediction of shear stress. Figure 14 shows the plot of the lowest RMSE generated from 1 to 50 neurons from ANN comprised of 1 and 2 hidden layers. It can be observed that one (1) hidden layer network generally outperforms two (2) hidden

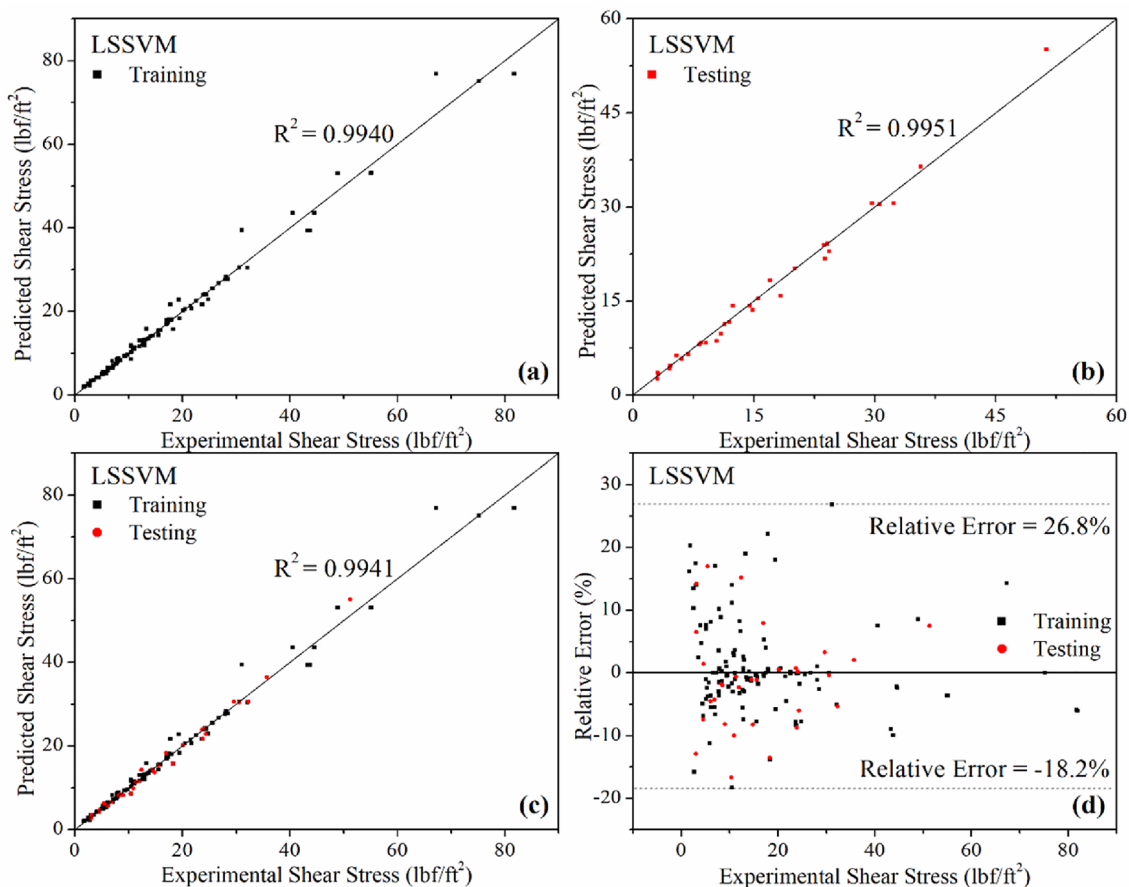


Fig. 13 Parity plots of LSSVM for prediction of shear stress: a Overall Data b Training Data c Testing Data; d Relative error of LSSVM for prediction of shear stress

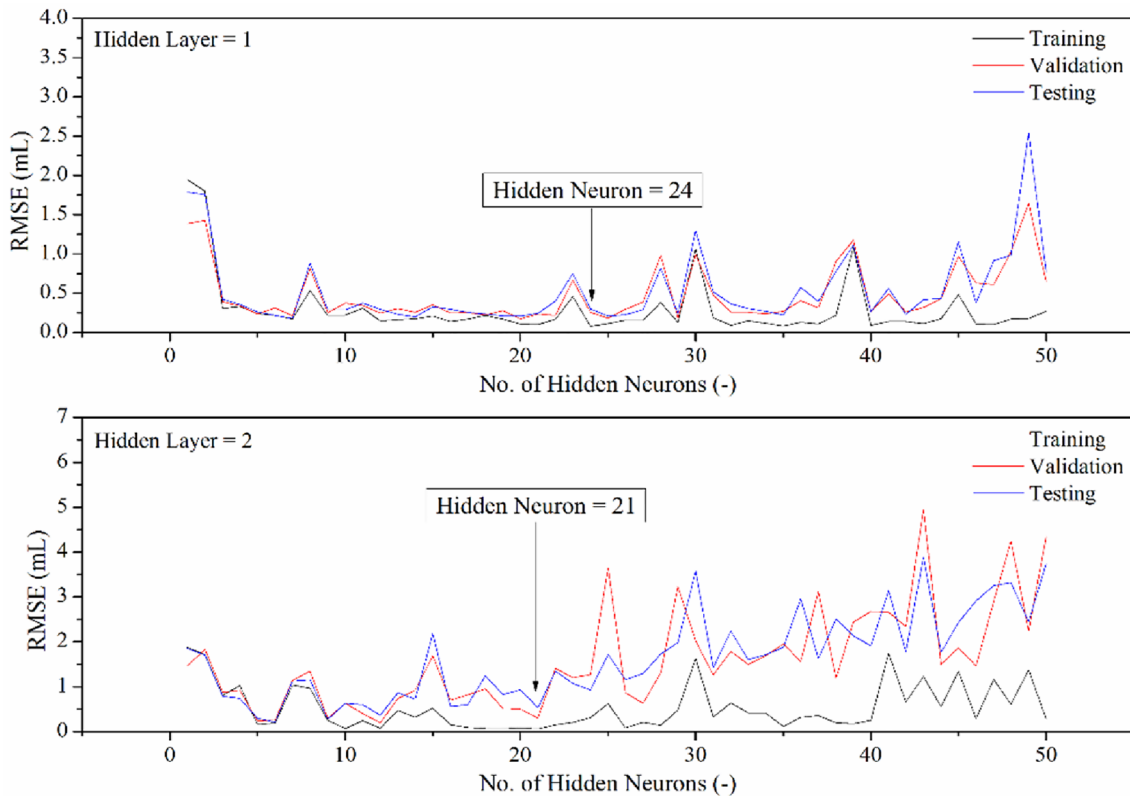


Fig. 14 RMSE of ANN for prediction of filtration volume

layers networks for the majority number of hidden nodes. As referred to Table 7, the network with (1) hidden layer and 24 hidden nodes yields the best prediction results with RMSE of 0.2103 mL and R^2 of 0.9993. Therefore, the final network architecture of ANN for prediction of filtration volume is determined to be 3–24–1.

The best validation performance is achieved with MSE of 0.04844 mL at epoch 15, as observed from Fig. 15. The RMSE computed based on the predicted outputs is 0.115 mL, 0.220 mL and 0.195 mL for the training, validation and testing datasets. As compared to the prediction of shear stress, the network for the prediction of filtration volume consumed more computation steps as the curves flatten after 18 epochs. The trendline of MSE before the tenth epoch indicates the network is prone to underfit as the MSE of the training vector is relatively high compared to the MSE after the fifteenth epoch.

Figure 16 shows the parity plots for different data environments. The predicted outputs are mostly overlying with the designated slope at $R^2 = 1$; this indicates that the prediction is highly accurate. The R^2 values for all the training, validation and testing are 0.9998, 0.9994 and 0.9993.

Table 7 Statistics of ANN predicted filtration volume for 1 and 2 hidden layers

Hidden layer	Prediction of filtration volume	
	1	2
Iteration	19	17
Hidden neuron	24	21
RMSE (Training), mL	0.0759	0.0555
RMSE (Validation), mL	0.2544	0.2995
RMSE (Testing), mL	0.3006	0.5352
R^2 (Training)	0.9999	1
R^2 (Validation)	0.9991	0.9979
R^2 (Testing)	0.9989	0.9968
Average RMSE, mL	0.2103	0.2967
Average R^2	0.9993	0.9982

According to Fig. 17, the relative errors of predicted output for filtration loss are relatively lower compared to the prediction of the shear rate as the maximum relative error lies between -12.7 and 23.5% .

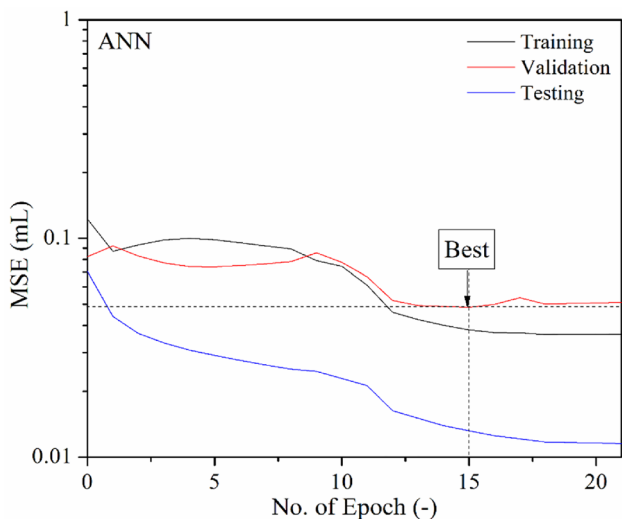


Fig. 15 MSE at different epochs of ANN for prediction of filtration volume

Least square support vector machine (LSSVM-FV)

The approach to select the kernel parameters in the prediction of shear stress is adopted in this section. Figure 18 shows that the 7th iteration yields the lowest RMSE with a value of 0.231 ml. The kernel and regularisation parameters at this iteration are $1.2484e + 08$ and 66.8216.

The computed RMSE values from the prediction of filtration volume using LSSVM are 0.2309 mL and 0.2308 mL for training and testing vectors. The R^2 values are 0.9992 and 0.9991 for the training and testing, respectively. The low RMSE and high R^2 obtained for all vectors demonstrate the capability of LSSVM with a low tendency to overfit or underfit in the training process. Lastly, the percentage of relative error for each predicted output corresponding to the actual value is calculated and plotted in the following figure. The relative error of the predicted filtration loss lies between -8.1 and 38.6%, as shown in Fig. 19.

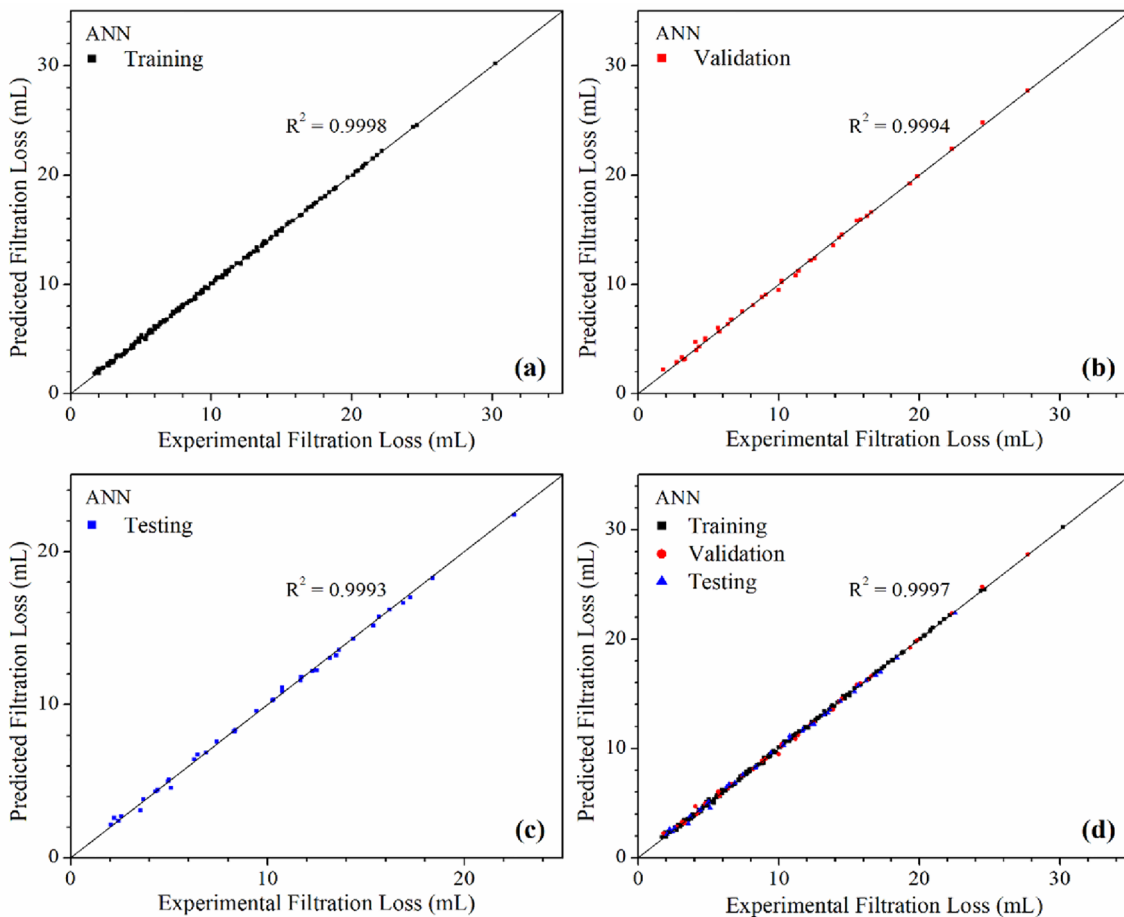


Fig. 16 Parity plots of ANN for prediction of filtration volume: **a** Overall Data **b** Training Data **c** Validation Data **d** Testing Data

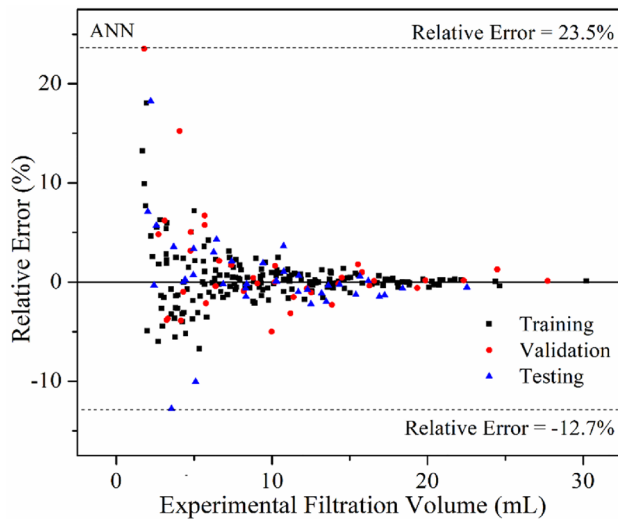


Fig. 17 Relative error of ANN for prediction of filtration volume

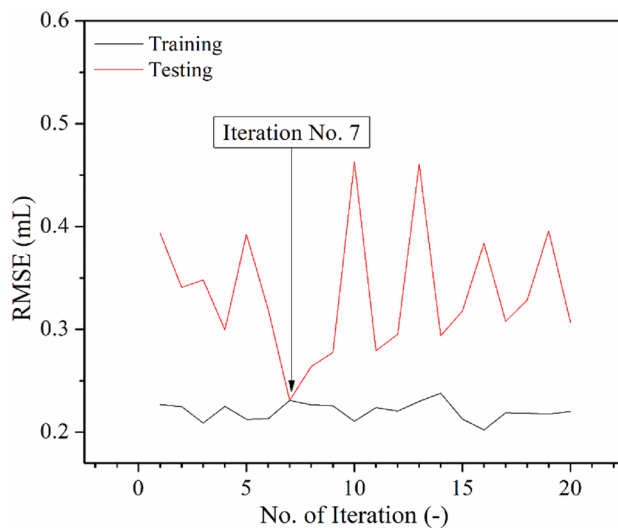


Fig. 18 RMSE of LSSVM for prediction of filtration volume

Analysis of outlier effect

Effect of outlier on the developed model is determined by analysing the William's plot. It is a graphical representation of standardised residuals (R) and leverage value. The leverage value variation in these plots is used to describe the outlier impact on model. Leverage values are defined as the data with extreme value of the predictor dataset (x). It is represented mathematically as Eq. (11).

$$H_i = x_i^T (X^T X)^{-1} x_i \quad (11)$$

where, H_i is the hat matrix (also known as projection matrix), x_i is the selected datapoint from the descriptive vector and X is the matrix from the training data descriptor values. The William's plot of all the developed models is presented in Fig. 20. Grubbs critical T value is used to separate the outlier from the valid data points on y-axis. It can be calculated using Eq. (12). The Grubbs critical T value for shear stress data is 3.91 and 4.05 for filtration volume data. The normalised leverage value is used in Fig. 20. Hence, the average of leverage is 1. Therefore, the leverage limit is arbitrarily selected the double of leverage average that is the value of 2 on x-axis. The leverage limit is used to separate high leverage value from the dataset. In Fig. 20, a square area is formed using Grubbs critical T value and leverage limit. This square area is known as applicability domain. The developed models are deemed a statistically valid model when most of the data are in this domain. As illustrated in this figure, majority of the datapoints are spotted in the applicability domain area which indicates that the models developed using ANN and LSSVM for shear stress and filtration volume prediction are reliable.

$$G = \frac{(n-1)}{\sqrt{n}} \sqrt{\frac{(t_{\alpha/(2n), n-3})^2}{n-3 + (t_{\alpha/(2n), n-3})^2}} \quad (12)$$

where, G is the Grubbs critical T value, $(n-3)$ is the degree of freedom and $\alpha/(2n)$ represents the significance level.

Comparison of ANN and LSSVM

Both applications of ANN and LSSVM showed acceptable and accurate results in predicting the shear stress and filtration loss of SiO_2 nanoparticles water-based drilling fluid. Table 8 and Table 9 summarise the RMSE, R^2 , MAE and MAPE of the developed model. Simulated results for all models achieved overall R^2 of minimum 0.990 with MAE and MAPE of not higher than 7%. Figure 21 illustrates the statistical parameters of ANN and LSSVM for further comparison.

Based on Table 8, the regression coefficient of ANN and LSSVM in the prediction of shear stress is 0.9937 and 0.9941, whereas the RMSE is 1.7235 lbf/ft² and 1.6003 lbf/ft², respectively. LSSVM model slightly outperforms ANN in predicting shear stress in terms of a higher R^2 and lower RMSE and MAPE. The R^2 of LSSVM is 0.04% higher than ANN, whereas the RMSE is 7.1% lower than ANN. According to Table 9, both models achieved an ideal prediction of filtration loss with R^2 of higher than 0.999. The comparison showed that the R^2 of ANN in the prediction of filtration volume is 0.05% higher than LSSVM, and RMSE is 33.7% lower than LSSVM. Hence, the prediction of ANN is more precise than LSSVM in predicting filtration loss.

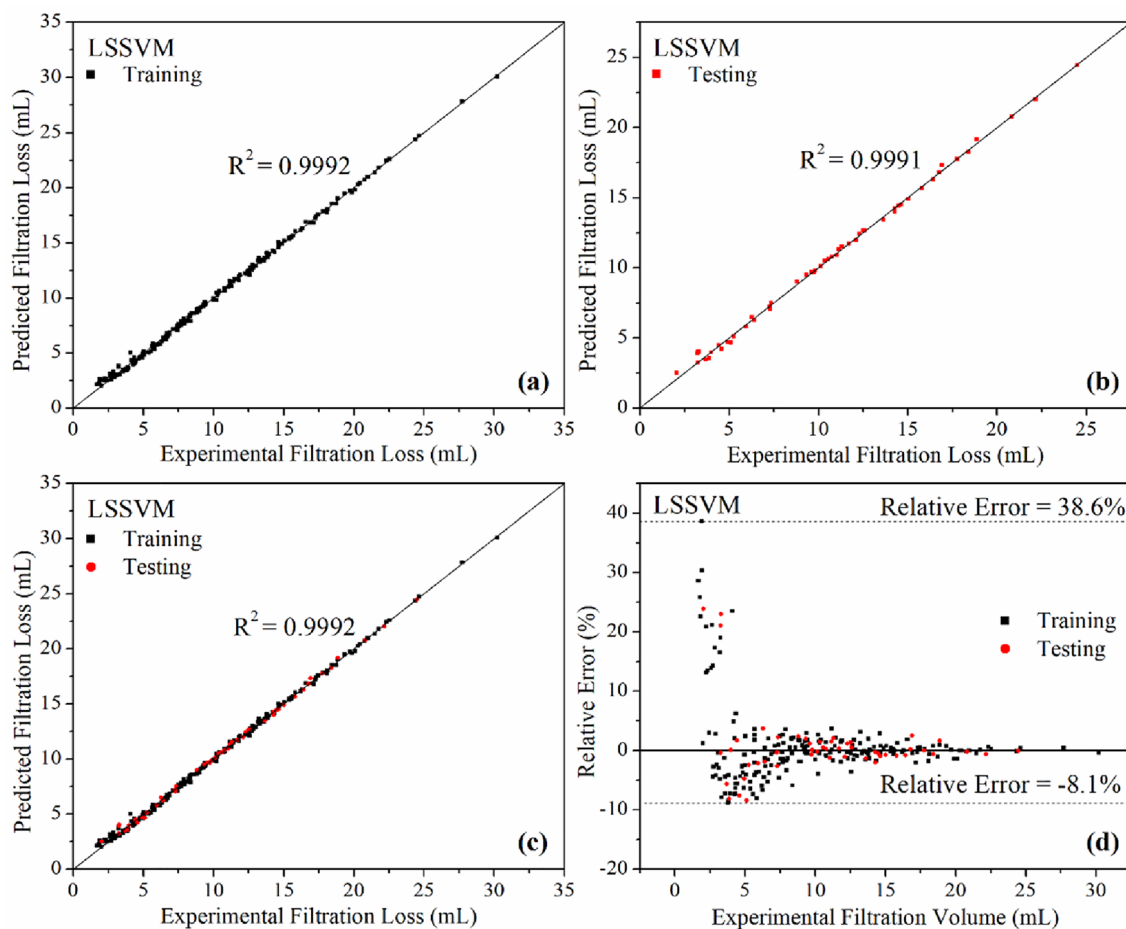


Fig. 19 Parity plots of LSSVM for prediction of filtration volume: **a** Overall Data **b** Training Data **c** Testing Data; **d** Relative error of LSSVM for prediction of filtration volume

Based on the analysis, both machine learning models are equally competent and capable of predicting the required parameters with high precision and accuracy. The accuracy of both machine learning models in predicting the filtration volume is generally higher than shear stress as indicated by all the statistics and the relative error distribution plot. One of the possible reasons could be due to a larger quantity of datasets available for the training.

Validation of the predicted outputs

The predicted output from the machine learning model with the best performance is plotted along with the corresponding experimental values to validate the trend of the predicted output. For the prediction of shear stress, predicted values from LSSVM is utilised in Fig. 22 as LSSVM performs better than the ANN. Figure 21 shows the rheo-grams of the SiO₂ nanoparticle WBM at 78°F and 140°F at varying nanoparticles concentration. Shear-thinning behaviour can be observed from both experimental and predicted trendlines

at all concentration of SiO₂. The magnitude or gradient of shear-thinning is more noticeable and significant at a higher SiO₂ nanoparticle concentration. This behaviour is favourable for a drilling fluid as low viscosity is preferred at a high shear rate to circulate the drilling fluid and cuttings. High viscosity at a low shear rate may ease the suspension of the drill cuttings during a drilling break.

The predicted filtration volume at 77 °F and 199 °F with a concentration ranging from 0 to 7.5 wt% is shown in Fig. 23. The predicted output from ANN is utilised in the plot as it has the best performance. The trend of both predicted and experimental output increases logarithmically with time, and filtration loss decreases with the increasing concentration of nanoparticles. The reduction in filtration loss can be justified by the nano-sized particles that can clog the pore throats on the filter paper compared to conventional drilling fluid particles.

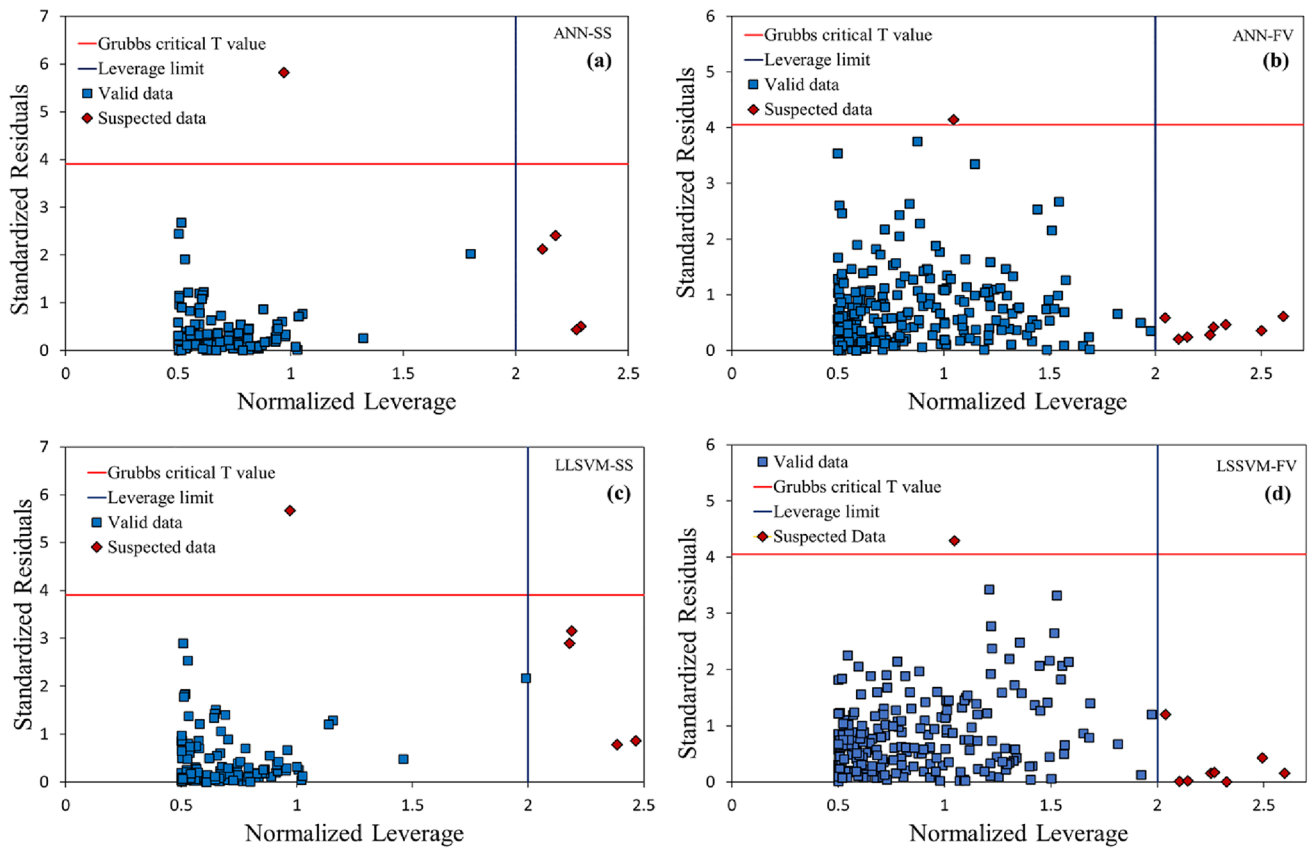


Fig. 20 William’s plots of ANN and LSSVM for prediction of shear stress (SS) and filtration volume (FV)

Table 8 Statistical results for prediction of shear stress

Prediction	Shear stress							
	ANN				LSSVM			
Methodology	R^2	RMSE (lbf/ft ²)	MAE (%)	MAPE (%)	R^2	RMSE (lbf/ft ²)	MAE (%)	MAPE (%)
Training	0.9930	2.0289	0.9286	6.1656	0.9940	1.6960	0.7899	4.3606
Validation	0.9981	0.4945	0.38174	4.5062	N/A	N/A	N/A	N/A
Testing	0.9992	0.4663	0.3061	2.7802	0.9951	1.2090	0.8297	6.1919
Overall	0.9937	1.7235	0.7562	5.4218	0.9941	1.6003	0.8047	5.0382

Table 9 Statistical results for prediction of filtration volume

Prediction	Filtration volume							
	ANN				LSSVM			
Methodology	R^2	RMSE (mL)	MAE (%)	MAPE (%)	R^2	RMSE (mL)	MAE (%)	MAPE (%)
Training	0.9998	0.1148	0.0514	0.9787	0.9992	0.2309	0.0909	1.9623
Validation	0.9994	0.2201	0.1655	2.9432	N/A	N/A	N/A	N/A
Testing	0.9993	0.1954	0.1470	2.4904	0.9991	0.2308	0.16839	2.9586
Overall	0.9997	0.1108	0.1099	1.1256	0.9992	0.1673	0.1020	2.0609

Fig. 21 Comparison of statistical parameters

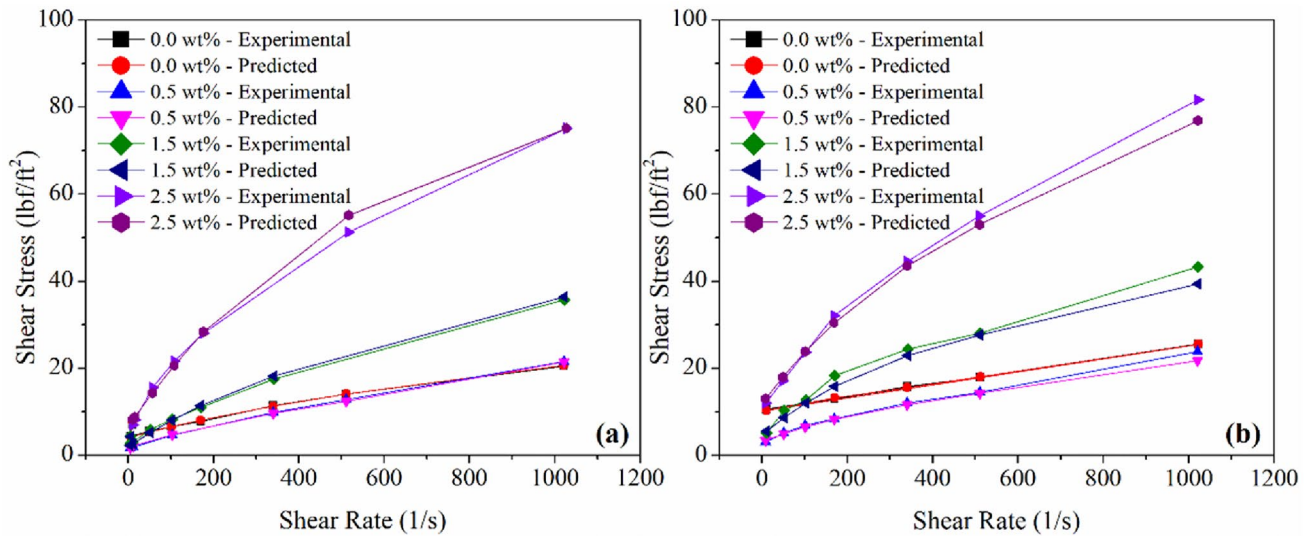
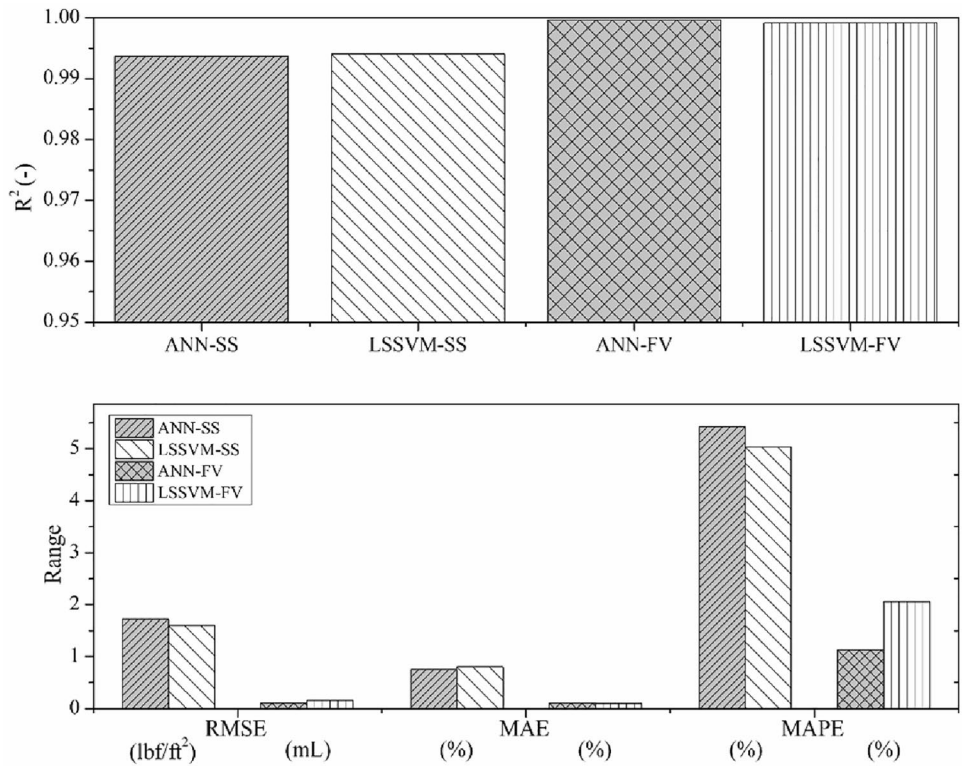


Fig. 22 Predicted and experimental rheo-gram. a 78 °F (b) 140 °F

Conclusions

Prediction of shear stress and filtration loss of SiO_2 nanoparticles water-based drilling fluid are accomplished by two machine learning-based approaches, i.e. ANN and LSSVM. The developed models demonstrate a well generalisation and a low tendency in overfitting. The predicted results for

both models achieved R^2 of higher than 0.99 and both MAE and MAPE not exceeding 7%. The RMSE for the predicted shear stress and filtration volume is lower than 1.8 lbf/ft^2 , and 0.2 mL, respectively. The following conclusions are deduced based on the predictive performance of developed ML models.

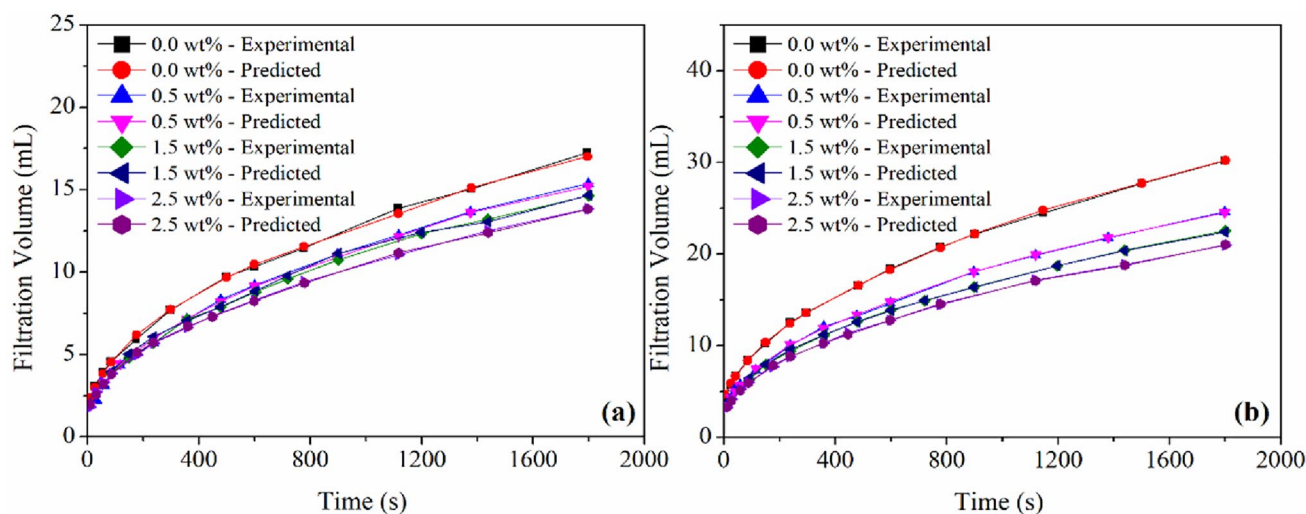


Fig. 23 Predicted and experimental filtration loss. **a** 77 °F **(b)** 199 °F

1. The assuring performances proved that both ANN and LSSVM are capable of predicting the output based on the precision of provided inputs.
2. It is found that LSSVM outperforms the ANN in the prediction of shear stress, whereas for the prediction of filtration volume, ANN performs better than the another. There is no definite conclusion of which machine learning approach is more superior in this research.
3. A shear-thinning behaviour is observed in the rheo-gram and a noticeable logarithmic increment of filtration loss with time.
4. The developed machine learning models are comprehensive and efficient in predicting the shear stress and filtration volume of a SiO₂ nanoparticles water-based drilling fluid.

Acknowledgements This research is fully supported by the Petroleum Engineering Department and Institute of Hydrocarbon recovery at Universiti Teknologi PETRONAS, Malaysia. The financial assistance is provided by Yayasan Universiti Teknologi PETRONAS (YUTP), grant number 015LC0-231.

Funding Funding was provided by Yayasan Universiti Teknologi PETRONAS (YUTP) (Grant Number 015LC0-231).

Declarations

Conflict of interest The authors declare that they have no known competing financial interests or personal relationships that could have appeared to influence the work reported in this paper.

Open Access This article is licensed under a Creative Commons Attribution 4.0 International License, which permits use, sharing, adaptation, distribution and reproduction in any medium or format, as long as you give appropriate credit to the original author(s) and the source, provide a link to the Creative Commons licence, and indicate if changes were made. The images or other third party material in this article are

included in the article's Creative Commons licence, unless indicated otherwise in a credit line to the material. If material is not included in the article's Creative Commons licence and your intended use is not permitted by statutory regulation or exceeds the permitted use, you will need to obtain permission directly from the copyright holder. To view a copy of this licence, visit <http://creativecommons.org/licenses/by/4.0/>.

References

- Abdo J, Haneef MD (2013) Clay nanoparticles modified drilling fluids for drilling of deep hydrocarbon wells. *Appl Clay Sci* 86:76–82. <https://doi.org/10.1016/j.clay.2013.10.017>
- Agarwal S, Tran P, Soong Y, et al (2011) Flow behaviour of nanoparticle stabilized drilling fluids and effect on high temperature aging. *AADE Natl Tech Conf Exhib* 1–6
- Agwu OE, Akpabio JU, Alabi SB, Dosunmu A (2018) Artificial intelligence techniques and their applications in drilling fluid engineering: a review. *J Pet Sci Eng* 167:300–315. <https://doi.org/10.1016/j.petrol.2018.04.019>
- Ahmadi MA (2016) Toward reliable model for prediction drilling fluid density at wellbore conditions: a LSSVM model. *Neurocomputing* 211:143–149. <https://doi.org/10.1016/j.neucom.2016.01.106>
- Alanazi AK, Alizadeh SM, Nurgalieva KS et al (2022) Application of neural network and time-domain feature extraction techniques for determining volumetric percentages and the type of two phase flow regimes independent of scale layer thickness. *Appl Sci* 12:1336. <https://doi.org/10.3390/app12031336>
- Al-Azani K, Elkatatny S, Ali A et al (2019) Cutting concentration prediction in horizontal and deviated wells using artificial intelligence techniques. *J Pet Explor Prod Technol* 9:2769–2779. <https://doi.org/10.1007/S13202-019-0672-3/FIGURES/17>
- Al-Khdheawi EA, Mahdi DS (2019) Apparent viscosity prediction of water-based muds using empirical correlation and an artificial neural network. *Energies* 12:3067. <https://doi.org/10.3390/en12163067>
- Alkinani HH, Al-Hameedi ATT, Dunn-Norman S (2020) Artificial neural network models to predict lost circulation in natural and induced fractures. *SN Appl Sci* 2:1–13. <https://doi.org/10.1007/S42452-020-03827-3/TABLES/6>

- Alvi MAA, Belayneh M, Saasen A, Aadnøy BS (2018) The effect of micro-sized boron nitride BN and iron trioxide Fe₂O₃ nanoparticles on the properties of laboratory bentonite drilling fluid. In: society of petroleum engineers-SPE, Norway one day seminar
- Al-Yasiri M, Wen D (2019) Gr-Al₂O₃ Nanoparticles-based multifunctional drilling fluid. *Ind Eng Chem Res* 58:10084–10091. <https://doi.org/10.1021/acs.iecr.9b00896>
- Aramendiz J, Imqam A (2020) Silica and graphene oxide nanoparticle formulation to improve thermal stability and inhibition capabilities of water-based drilling fluid applied to woodford shale. *SPE Drill Complet* 35:164–179. <https://doi.org/10.2118/193567-PA>
- Asadi A, Alarifi IM, Nguyen HM, Moayed H (2021) Feasibility of least-square support vector machine in predicting the effects of shear rate on the rheological properties and pumping power of MWCNT–MgO/oil hybrid nanofluid based on experimental data. *J Therm Anal Calorim* 143:1439–1454. <https://doi.org/10.1007/s10973-020-09279-6>
- Barati-Harooni A, Najafi-Marghmaleki A, Tatar A et al (2016) Prediction of frictional pressure loss for multiphase flow in inclined annuli during underbalanced drilling operations. *Nat Gas Ind B* 3:275–282. <https://doi.org/10.1016/j.ngib.2016.12.002>
- Bello O, Holzmann J, Yaqoob T, Teodoru C (2015) Application of artificial intelligence methods in drilling system design and operations: a review of the state of the art. *J Artif Intell Soft Comput Res* 5:121–139. <https://doi.org/10.1515/jaiscr-2015-0024>
- Cai J, Chenevert MEE, Sharma MMM, Friedheim J (2012) Decreasing water invasion into atoka shale using nonmodified silica nanoparticles. *SPE Drill Complet* 27:103–112. <https://doi.org/10.2118/146979-PA>
- Chen L, Duan L, Shi Y, Du C (2020) PSO_LSSVM prediction model and its MATLAB implementation. *IOP Conf Ser Earth Environ Sci* 428:012089. <https://doi.org/10.1088/1755-1315/428/1/012089>
- Cheraghian G, Wu Q, Mostofi M et al (2018) Effect of a novel clay/silica nanocomposite on water-based drilling fluids: improvements in rheological and filtration properties. *Colloids Surfaces A Physicochem Eng Asp* 555:339–350. <https://doi.org/10.1016/j.colsurfa.2018.06.072>
- Cohen IL (1994) An artificial neural network analogue of learning in autism. *Biol Psychiatry* 36:5–20. [https://doi.org/10.1016/0006-3223\(94\)90057-4](https://doi.org/10.1016/0006-3223(94)90057-4)
- Contreras O, Hareland G, Husein M, et al (2014) Application of in-house prepared nanoparticles as filtration control additive to reduce formation damage. In: SPE - European formation damage conference, proceedings, EFDC
- da Bispo VDS, Scheid CM, Calçada LA, da Meleiro LA, C (2017) Development of an ANN-based soft-sensor to estimate the apparent viscosity of water-based drilling fluids. *J Pet Sci Eng* 150:69–73. <https://doi.org/10.1016/j.petrol.2016.11.030>
- Dashti A, Raji M, Alivand MS, Mohammadi AH (2020) Estimation of CO₂ equilibrium absorption in aqueous solutions of commonly used amines using different computational schemes. *Fuel* 264:116616. <https://doi.org/10.1016/j.fuel.2019.116616>
- Du Y-C, Stephanus A (2018) Levenberg-marquardt neural network algorithm for degree of arteriovenous fistula stenosis classification using a dual optical photoplethysmography sensor. *Sensors* 18:2322. <https://doi.org/10.3390/s18072322>
- Einstein A (1906) Eine neue bestimmung der moleküldimensionen. *Ann Phys* 324:289–306. <https://doi.org/10.1002/andp.19063240204>
- Gbadamosi AO, Junin R, Abdalla Y et al (2019) Experimental investigation of the effects of silica nanoparticle on hole cleaning efficiency of water-based drilling mud. *J Pet Sci Eng* 172:1226–1234. <https://doi.org/10.1016/j.petrol.2018.09.097>
- Ghanbari S, Kazemzadeh E, Soleymani M, Naderifar A (2016) A facile method for synthesis and dispersion of silica nanoparticles in water-based drilling fluid. *Colloid Polym Sci* 294:381–388. <https://doi.org/10.1007/s00396-015-3794-2>
- Ghorbani H, Wood DA, Choubineh A et al (2020) Performance comparison of bubble point pressure from oil PVT data: several neurocomputing techniques compared. *Exp Comput Multiph Flow* 2:225–246. <https://doi.org/10.1007/s42757-019-0047-5>
- Golsefatan A, Shahbazi K (2021) Predicting performance of SiO₂ nanoparticles on filtration volume using reliable approaches: application in water-based drilling fluids. *Energy Sources, Part A Recover Util Environ Eff* 43:3216–3225. <https://doi.org/10.1080/15567036.2019.1639854>
- Gomaa I, Elkhatatny S, Abdurraheem A (2020) Real-time determination of rheological properties of high over-balanced drilling fluid used for drilling ultra-deep gas wells using artificial neural network. *J Nat Gas Sci Eng* 77:103224. <https://doi.org/10.1016/j.jngse.2020.103224>
- Gowida A, Elkhatatny S, Ramadan E, Abdurraheem A (2019) Data-driven framework to predict the rheological properties of CaCl₂ brine-based drill-in fluid using artificial neural network. *Energies* 12:1880. <https://doi.org/10.3390/en12101880>
- Kang Y, She J, Zhang H et al (2016) Strengthening shale wellbore with silica nanoparticles drilling fluid. *Petroleum* 2:189–195. <https://doi.org/10.1016/j.petlm.2016.03.005>
- Keshavarz Moraveji M, Ghaffarkhah A, Agin F et al (2020) Application of amorphous silica nanoparticles in improving the rheological properties, filtration and shale stability of glycol-based drilling fluids. *Int Commun Heat Mass Transf* 115:104625. <https://doi.org/10.1016/j.icheatmasstransfer.2020.104625>
- Liu T-Y, Zhang P, Wang J, Ling Y-F (2020) Compressive strength prediction of PVA fiber-reinforced cementitious composites containing nano-SiO₂ using BP neural network. *Mater (basel)* 13:521. <https://doi.org/10.3390/ma13030521>
- Ma X, Zhang Y, Cao H et al (2018) Nonlinear regression with high-dimensional space mapping for blood component spectral quantitative analysis. *J Spectrosc* 2018:1–8. <https://doi.org/10.1155/2018/2689750>
- Maghrabi S, Kulkarni D, Teke K, et al (2014) Modeling of shale-erosion behavior in aqueous drilling fluids. In: society of petroleum engineers-European unconventional resources conference and exhibition 2014: unlocking European potential
- Mahmoud O, Nasr-El-Din HA, Vryzas Z, Kelessidis VC (2018) Using ferric oxide and silica nanoparticles to develop modified calcium bentonite drilling fluids. *SPE Drill Complet* 33:12–26. <https://doi.org/10.2118/178949-PA>
- Mahmoud O, Nasr-El-Din HA, Vryzas Z, Kelessidis VC (2016) Nanoparticle-based drilling fluids for minimizing formation damage in HP/HT applications. In: SPE international formation damage control symposium proceedings
- Maiti M, Ranjan R, Chaturvedi E et al (2021) Formulation and characterization of water-based drilling fluids for gas hydrate reservoirs with efficient inhibition properties. *J Dispers Sci Technol* 42:338–351. <https://doi.org/10.1080/01932691.2019.1680380>
- Mao H, Qiu Z, Shen Z, Huang W (2015) Hydrophobic associated polymer based silica nanoparticles composite with core-shell structure as a filtrate reducer for drilling fluid at ultra-high temperature. *J Pet Sci Eng* 129:1–14. <https://doi.org/10.1016/j.petrol.2015.03.003>
- Masoumi N, Sohrabi N, Behzadmehr A (2009) A new model for calculating the effective viscosity of nanofluids. *J Phys D Appl Phys* 42:055501. <https://doi.org/10.1088/0022-3727/42/5/055501>
- Medhi S, Chowdhury S, Kumar A et al (2020) Zirconium oxide nanoparticle as an effective additive for non-damaging drilling fluid: a study through rheology and computational fluid dynamics investigation. *J Pet Sci Eng* 187:106826. <https://doi.org/10.1016/j.petrol.2019.106826>
- Meybodi MK, Naseri S, Shokrollahi A, Daryasafar A (2015) Prediction of viscosity of water-based Al₂O₃, TiO₂, SiO₂, and CuO

- nanofluids using a reliable approach. *Chemom Intell Lab Syst* 149:60–69. <https://doi.org/10.1016/j.chemolab.2015.10.001>
- Milad Arabloo AS (2014) Application of SVM algorithm for frictional pressure loss calculation of three phase flow in inclined annuli. *J Pet Environ Biotechnol*. <https://doi.org/10.4172/2157-7463.1000179>
- Moratis L (2016) Out of the ordinary? Appraising ISO 26000's CSR definition. *Int J Law Manag* 58:26–47. <https://doi.org/10.1108/IJLMA-12-2014-0064>
- Osman EA, Aggour MA (2003) Determination of drilling mud density change with pressure and temperature made simple and accurate by ANN. *Proc Middle East Oil Show* 13:115–126. <https://doi.org/10.2118/81422-MS>
- Ozbayoglu ME, Ozbayoglu MA (2007) Flow pattern and frictional-pressure-loss estimation using neural networks for UBD operations. *IADC/SPE Manage Press Drill Underbalanced Oper One-Petro*. <https://doi.org/10.2118/108340-MS>
- Parizad A, Shahbazi K, Tanha AA (2018) SiO₂ nanoparticle and KCl salt effects on filtration and thixotropic behavior of polymeric water based drilling fluid: with zeta potential and size analysis. *Result Phys* 9:1656–1665. <https://doi.org/10.1016/j.rinp.2018.04.037>
- Popa AS, Cassidy S (2012) Artificial intelligence for heavy oil assets: the evolution of solutions and organization capability. In: proceedings-SPE annual technical conference and exhibition
- Razi MM, Mazidi M, Razi FM et al (2013) Artificial neural network modeling of plastic viscosity, yield point, and apparent viscosity for water-based drilling fluids. *J Dispers Sci Technol* 34:822–827. <https://doi.org/10.1080/01932691.2012.704746>
- Riley M, Stamatakis E, Young S, et al (2012) Wellbore stability in unconventional shale-the design of a nano-particle fluid. In: society of petroleum engineers-SPE oil and gas india conference and exhibition 2012, OGIC-further, deeper, tougher: the quest continues...
- Sadegh Hassani S, Amrollahi A, Rashidi A et al (2016) The effect of nanoparticles on the heat transfer properties of drilling fluids. *J Pet Sci Eng* 146:183–190. <https://doi.org/10.1016/j.petrol.2016.04.009>
- Safari H, Shokrollahi A, Jamialahmadi M et al (2014) Prediction of the aqueous solubility of BaSO₄ using pitzer ion interaction model and LSSVM algorithm. *Fluid Phase Equilib* 374:48–62. <https://doi.org/10.1016/j.fluid.2014.04.010>
- Sapna S (2012) Backpropagation learning algorithm based on levenberg marquardt algorithm. in: computer science and information technology (CS & IT). *Acad Ind Res Collab Cent (AIRCC)* 2:393–398
- Shadravan A, Tarrahi M, Amani M (2015) Intelligent tool to design fracturing, drilling, spacer and cement slurry fluids using machine learning algorithms. In: society of petroleum engineers-SPE Kuwait Oil and Gas show and conference
- Shahsavari A, Bagherzadeh SA, Mahmoudi B et al (2019) Robust weighted least squares support vector regression algorithm to estimate the nanofluid thermal properties of water/graphene oxide-silicon carbide mixture. *Phys A Stat Mech Its Appl* 525:1418–1428. <https://doi.org/10.1016/j.physa.2019.03.086>
- Smith SR, Rafati R, Sharifi Haddad A et al (2018) Application of aluminium oxide nanoparticles to enhance rheological and filtration properties of water based muds at HPHT conditions. *Colloids Surfaces A Physicochem Eng Asp* 537:361–371. <https://doi.org/10.1016/j.colsurfa.2017.10.050>
- Tanoumand N, Hemmati-Sarapardeh A, Bahadori A (2015) A CSA-LSSVM Model to estimate diluted heavy oil viscosity in the presence of kerosene. *Pet Sci Technol* 33:1085–1092. <https://doi.org/10.1080/10916466.2015.1034367>
- Tomiwa O, Oluwatosin R, Temiloluwa O, et al (2019) Improved water based mud using Solanum tuberosum formulated biopolymer and application of artificial neural network in predicting mud rheological properties. In: society of petroleum engineers-SPE Nigeria annual international conference and exhibition 2019, NAIC 2019
- Udawatha DS, Narayana M, Wijayarathne UPL (2019) Predicting the effective viscosity of nanofluids based on the rheology of suspensions of solid particles. *J King Saud Univ - Sci* 31:412–426. <https://doi.org/10.1016/j.jksus.2017.09.016>
- Uma Maheswari R, Umamaheswari R (2020) Adaptive data-driven nonlinear synchro squeezed transform with single class radial basis function kernel support vector machine applied to wind turbine planetary gearbox fault diagnostics. *Proc Inst Mech Eng Part A J Power Energy*. <https://doi.org/10.1177/0957650919886227>
- Vargas J, Roldán LJ, Lopera SH, et al (2020) Effect of silica nanoparticles on thermal stability in bentonite free water-based drilling fluids to improve its rheological and filtration properties after aging process. In: offshore technology conference Brasil 2019, OTCB 2019
- Vryzas Z, Mahmoud O, Nasr-El-din HA, Kelessidis VC (2015) Development and testing of novel drilling fluids using Fe₂O₃ and SiO₂ nanoparticles for enhanced drilling operations. In: international petroleum technology conference, IPTC 2015
- Wang H, Hu D (2005) Comparison of SVM and LS-SVM for regression. In: proceedings of 2005 international conference on neural networks and brain proceedings, ICNNB'05
- Yu H, Wilamowski BM (2018) Levenberg-marquardt training. In: Bogdan M, Wilamowski J, David I (eds) intelligent systems. CRC Press
- Zakaria MF, Husein M, Hareland G (2012) Novel nanoparticle-based drilling fluid with improved characteristics. In: society of petroleum engineers-SPE international oilfield nanotechnology conference 2012

Publisher's Note Springer Nature remains neutral with regard to jurisdictional claims in published maps and institutional affiliations.